IRF4 haploinsufficiency in a family with Whipple's disease

Antoine Guerin, Gaspard Kerner, Nico Marr, Janet G. Markle, Florence Fenollar, Natalie Wong, Sabri Boughorbel, Danielle T. Avery, Cindy S. Ma, Salim Bougarn, et al.

IRF4 haploinsufficiency in a family with Whipple's disease

Antoine Guérin, Ph.D.,[1,2] Gaspard Kerner, M.Sc.,[1,2,*] Nico Marr, Ph.D.,[3,*]
Janet G. Markle, Ph.D.,[4,§] Florence Fenollar, M.D., Ph.D.,[5,§] Natalie Wong, B. Sc. (Hons),[6,7,§]
Sabri Boughorbel, Ph.D.,[3,§] Danielle T. Avery, B. Sc.,[6,7,§] Cindy S. Ma, Ph.D.,[6,7,§]
Salim Bougarn, Ph.D.,[3,§] Matthieu Bouaziz, Ph.D.,[1,2] Vivien Béziat, Ph.D.,[1,2]
Erika Della Mina, Ph.D.,[1,2] Carmen Oleaga-Quintas, M.Sc.,[1,2] Tomi Lazarov, B.Sc.,[8]
Lisa Worley, B.Sc. (Hons),[6,7] Tina Nguyen, B.Sc. (Hons),[6,7] Etienne Patin, Ph.D.,[9,10,11]
Caroline Deswarte, M.Sc.,[1,2] Rubén Martinez-Barricarte, Ph.D.,[4] Soraya Boucherit, M.D.,[1,2]
Xavier Ayral, M.D.,[12] Sophie Edouard, PharmD.,[5] Stéphanie Boisson-Dupuis, Ph.D.,[1,2,4]
Vimel Rattina, M.Sc.,[1,2] Benedetta Bigio, M.Sc.,[4] Guillaume Vogt, Ph.D.,[2]
Frédéric Geissmann, M.D., Ph.D.,[8,13,°] Lluis Quintana-Murci, Ph.D.,[9,10,11,°]
Damien Chaussabel, Ph.D.,[3,°] Stuart G. Tangye, Ph.D.,[6,7,°] Didier Raoult, M.D., Ph.D.,[5,#]
Laurent Abel, M.D., Ph.D.,[1,2,4,#] Jacinta Bustamante, M.D., Ph.D.,[1,2,4,14,#]
and Jean-Laurent Casanova, M.D., Ph.D.,[1,2,4,15,16,#,@]

1. Laboratory of Human Genetics of Infectious Diseases, Necker Branch, INSERM U1163, 75015 Paris, France, EU.
2. Paris Descartes University, Imagine Institute, 75015 Paris, France, EU.
3. Sidra Medical and Research Center, Doha, Qatar.
4. St. Giles Laboratory of Human Genetics of Infectious Diseases, Rockefeller Branch, The Rockefeller University, New York, NY 10065, USA.
5. Research Unit of Infectious and Tropical Emerging Diseases, University Aix-Marseille, URMITE, UM63, CNRS 7278, IRD 198, 13005 Marseille, France, EU.
6. Immunology Division, Garvan Institute of Medical Research, Darlinghurst, NSW 2010, Australia.
7. St Vincent's Clinical School, Faculty of Medicine, UNSW Sydney NSW 2010, Australia.
8. Immunology Program and Ludwig Center, Memorial Sloan Kettering Cancer Center, New York, NY 10065, USA.
9. Human Evolutionary Genetics Unit, Department of Genomes & Genetics, Institut Pasteur, Paris 75015, France, EU.
10. CNRS UMR2000, 75015 Paris, France, EU.
11. Center of Bioinformatics, Biostatistics and Integrative Biology, Institut Pasteur, 75015 Paris, France, EU.
12. Rheumatology Unit, Cochin Hospital, 75014 Paris, France, EU.
13. Weill Cornell Graduate School of Medical Sciences, New York, NY 10065, USA.
14. Center for the Study of Primary Immunodeficiencies, Assistance Publique-Hôpitaux de Paris, Necker Hospital for Sick Children, 75015 Paris, France, EU.
15. Pediatric Hematology and Immunology Unit, Assistance Publique-Hôpitaux de Paris, Necker Hospital for Sick Children, 75015 Paris, France, EU.
16. Howard Hughes Medical Institute, New York, NY 10065 USA.

*,§,°,# Equal contributions

@ Correspondence: casanova@rockefeller.edu

Keywords: Whipple's disease, primary immunodeficiency, IRF4, haploinsufficiency

Running title: Whipple's disease and IRF4 deficiency

Conflict of interest statement: The authors have no conflict of interest to declare.

Abstract

Most humans are exposed to *Tropheryma whipplei* (Tw). Whipple's disease (WD) strikes only a small minority of individuals infected with Tw (<0.01%), whereas asymptomatic chronic carriage is more common (<25%). We studied a multiplex kindred, containing four WD patients and five healthy Tw chronic carriers. We hypothesized that WD displays autosomal dominant (AD) inheritance, with age-dependent incomplete penetrance. We identified a single very rare non-synonymous mutation in the four patients: the private R98W variant of IRF4, a transcription factor involved in immunity. The five Tw carriers were younger, and also heterozygous for R98W. We found that R98W was loss-of-function, modified the transcriptome of heterozygous leukocytes following Tw stimulation, and was not dominant-negative. We also found that only six of the other 153 known non-synonymous IRF4 variants were loss-of-function. Finally, we found that *IRF4* had evolved under purifying selection. AD IRF4 deficiency can underlie WD by haploinsufficiency, with age-dependent incomplete penetrance.

Introduction

Whipple's disease (WD) was first described as an intestinal inflammatory disease by George H. Whipple in 1907 (Whipple, 1907). Its infectious origin was suspected in 1961 (Yardley and Hendrix, 1961), and the causal microbe, *Tropheryma whipplei* (Tw), a Gram-positive actinomycete, was detected by PCR in 1992 (Relman et al., 1992), and cultured in 2000 (Raoult et al., 2000). Tw is probably transmitted between humans via the oro-oral or feco-oral routes. WD is a chronic condition with a late onset (mean age at onset: 55 years) (Braubach et al., 2017) affecting multiple organs. The clinical manifestations of classical WD are arthralgia, diarrhea, abdominal pain, and weight loss (Dobbins, 1987; Durand et al., 1997; Fleming et al., 1988; Mahnel et al., 2005; Maizel et al., 1970). However, about 25% of WD patients display no gastrointestinal or osteoarticular symptoms, instead presenting with cardiac and/or neurological manifestations (Durand et al., 1997; Fenollar et al., 2014; Fenollar et al., 2001; Gubler et al., 1999; Schneider et al., 2008). WD is fatal if left untreated, and relapses occur in 2 to 33% of treated cases, even after prolonged appropriate antibiotic treatment (Lagier et al., 2011; Marumganti and Murphy, 2008). WD is rare and has been estimated to affect about one in a million individuals (Dobbins, 1981; Dobbins, 1987; Fenollar et al., 2007). However, about two thousand cases have been reported in at least nine countries worldwide, mostly in North America and Western Europe (Bakkali et al., 2008; Desnues et al., 2010; Fenollar et al., 2008a; Lagier et al., 2010; Puechal, 2016; Schneider et al., 2008). Chronic asymptomatic carriage of Tw is common in the general population, and this bacterium has been detected in feces, saliva, and intestinal mucosae. The prevalence of Tw carriage in the feces has been estimated at 2 to 11% for the general population, but can reach 26% in sewer workers and 37% in relatives of patients and carriers (Amsler et al., 2003; Ehrbar et al., 1999; Fenollar et al., 2014; Fenollar et al., 2007; Maibach et al., 2002; Rolain et al., 2007; Schneider et al., 2008; Street et al., 1999).

Seroprevalence for specific antibodies against Tw in the general population varies from 50% in France to 70% in Senegal (Fenollar et al., 2009; Fenollar et al., 2014; Raoult et al., 2000; Schneider et al., 2008). At least 75% of infected individuals clear Tw primary infections, but a minority (<25%) become asymptomatic carriers, a very small proportion of whom develop WD (<0.01%) (Fenollar et al., 2008b). Tw infection is, therefore, necessary, but not sufficient, for WD development, and it is unclear whether prolonged asymptomatic carriage necessarily precedes WD. The hypothesis that WD results from the emergence of a more pathogenic clonal strain of Tw was not supported by bacterial genotyping (Li et al., 2008). WD mostly affects individuals of European origin, but does not seem to be favored by specific environments. WD is typically sporadic, but six multiplex kindreds have been reported, with cases often diagnosed years apart, suggesting a possible genetic component (Durand et al., 1997; Fenollar et al., 2007; Ponz de Leon et al., 2006). WD patients are not prone to other severe infections (Marth et al., 2016). Moreover, WD has never been reported in patients with conventional primary immunodeficiencies (PIDs) (Picard et al., 2018). This situation is reminiscent of other sporadic severe infections, such as herpes simplex virus-1 encephalitis, severe influenza, recurrent rhinovirus infection, severe varicella zoster disease, trypanosomiasis, invasive staphylococcal disease, and viral infections of the brainstem, which are caused by single-gene inborn errors of immunity in some patients (Andersen et al., 2015; Casanova, 2015a; Casanova, 2015b; Ciancanelli et al., 2015; Israel et al., 2017; Lamborn et al., 2017; Lenardo et al., 2016; Ogunjimi et al., 2017; Vanhollebeke et al., 2006; Zhang et al., 2018). We therefore hypothesized that WD might be due to monogenic inborn errors of immunity to Tw, with age-dependent incomplete penetrance.

Results

A multiplex kindred with WD

We investigated four related patients diagnosed with WD (P1, P2, P3, and P4) with a mean age at diagnosis of 58 years. They belong to a large non-consanguineous French kindred (Figure 1A). The proband (P1), a 69-year-old woman, presented with right knee arthritis in 2011, after recurrent episodes of arthritis of the right knee since 1980. Tw was detected in the synovial fluid by PCR and culture, but not in saliva, feces, or small intestine tissue by PCR. Treatment with doxycycline and hydroxychloroquine was effective. At last follow-up, in 2016, P1 was well and Tw PCR on saliva and feces was negative. P2, a second cousin of P1, is a 76-year-old woman with classical WD diagnosed at 37 years of age in 1978 by periodic acid–Schiff (PAS) staining of a small intestine biopsy specimen. She was treated with sulfamethoxazole/trimethoprim. At last follow-up, in 2016, Tw PCR on saliva and feces was positive. P3, the father of P1, is a 92-year-old man with classical WD diagnosed at 62 years of age, in 1987, based on positive PAS staining of a small intestine biopsy specimen. Long-term sulfamethoxazole/trimethoprim treatment led to complete clinical and bacteriological remission. P4, the brother of P2, is a 70-year-old man who consulted in 2015 for arthralgia of the knees and right ulna-carpal joints. PCR and culture did not detect Tw in saliva and feces, but serological tests for Tw were positive. Treatment with methotrexate and steroids was initiated before antibiotics, the effect of which is currently being evaluated. All four patients are otherwise healthy. Saliva and/or feces samples from 18 other members of the family were tested for Tw (Figure 1A; Figure 1-source data 1). Five individuals are chronic carriers (mean age: 55 years) and 13 tested negative (mean age: 38 years). Nine additional relatives could not be tested. The distribution of WD in this kindred was suggestive of an AD trait with incomplete clinical penetrance.

A private heterozygous missense *IRF4* variant segregates with WD

We analyzed the familial segregation of WD by genome-wide linkage (GWL), using information from both genome-wide single-nucleotide polymorphism (SNP) microarrays and whole-exome sequencing (WES) (Belkadi et al., 2016). Multipoint linkage analysis was performed under an AD model, with a very rare disease-causing allele ($<10^{-5}$) and age-dependent incomplete penetrance. Twelve chromosomal regions linked to WD were identified on chromosomes 1 (x3), 2, 3, 6, 7, 8, 10, 11, 12 and 17, with a LOD score close (>1.90) to the maximum expected value (1.95) (Figure 1-figure supplement 1A). These regions covered 27.18 Mb and included 263 protein-coding genes. WES data analysis for these 263 genes identified 54 heterozygous non-synonymous coding variants common to all four WD patients (Figure 1-source data 2). Only one, a variant of the Interferon regulatory factor (*IRF*) 4 gene encoding a transcription factor from the IRF family (Ikushima et al., 2013), located in a 200 kb linked region on chromosome 6 (Figure 1-figure supplement 1A, 1B), was very rare, and was even found to be private [not found in the gnomAD database, http://gnomad.broadinstitute.org, or in our in-house WES database (HGID)], whereas all other variants had a frequency >0.001, which is inconsistent with the frequency of WD and our hypothesis of a very rare ($<10^{-5}$) deleterious heterozygous allele. The variant is a c.292 C>T substitution in exon 3 of *IRF4,* replacing the arginine residue in position 98 with a tryptophan residue (R98W) (Figure 1A, 1B, 1C). IRF4 is a transcription factor with an important pleiotropic role in innate and adaptive immunity, at least in a few strains of inbred mice (Shaffer et al., 2009). Mice heterozygous for a null *Irf4* mutation have not been studied, but homozygous null mice have various T- and B-cell abnormalities and are susceptible to both *Leishmania* and lymphocytic choriomeningitis virus (Klein et al., 2006; Lohoff et al., 2002; Mittrucker et al., 1997; Suzuki et al., 2004; Tamura et al., 2005; Tominaga et al., 2003). We

confirmed the *IRF4* R98W mutation by Sanger sequencing genomic DNA from the blood of the four WD patients (Figure 1C). Thirteen relatives of the WD patients were WT/WT at the *IRF4* locus, and 10 of these relatives (77%) tested negative for Tw carriage. Eight other relatives were heterozygous for the *IRF4* R98W mutation, five of whom (62.5%) were Tw carriers (mean age: 55 years) (Figure 1A; Figure 1-source data 1). Overall, 12 individuals from the kindred, including the four patients, the five chronic carriers of Tw, two non-carriers of Tw and one relative not tested for Tw, were heterozygous for *IRF4* R98W (Figure 1A; Figure 1-source data 1). The familial segregation of the *IRF4* R98W allele was therefore consistent with an AD pattern of WD inheritance with incomplete clinical penetrance. Chronic Tw carriage also followed an AD mode of inheritance.

R98W is predicted to be loss-of-function, unlike most other IRF4 variants

The R98 residue in the DNA-binding domain (DBD) of IRF4 is highly conserved in the 12 species for which *IRF4* has been sequenced (Figure 1B, 1D). It has been suggested that this residue is essential for IRF4 DNA-binding activity, because the R98A-C99A double mutant is loss-of-function (Brass et al., 1999; Escalante et al., 2002). The R98W mutation is predicted to be damaging by multiple programs (Kircher et al., 2014); it has a CADD score of R98W (26.5), well above the mutation significance cutoff (MSC) of IRF4 (11.125) (Figure 2) (Itan et al., 2016; Kircher et al., 2014). The R98W variant was not present in the gnomAD database or our in-house HGID database of more than 4,000 WES from patients with various infectious diseases. The mutant allele was not found in the sequences for the CEPH-HGDP panel of 1,052 controls from 52 ethnic groups, or in 100 French controls, confirming that this variant was very rare, probably private to this kindred. Therefore, the minor allele frequency (MAF) of this private allele is $<4x10^{-6}$. Moreover, the *IRF4* gene has a gene damage index (GDI) of 2.85, a neutrality index score of 0.15 (Itan et al., 2015), and a purifying selection *f*

parameter of 0.32 (among the <10% of genes in the genome subject to the greatest constraint; Figure 2-figure supplement 1), strongly suggesting that *IRF4* has evolved under purifying selection (i.e., strong evolutionary constraints) (Eilertson et al., 2012). Biologically disruptive heterozygous mutations of *IRF4* are therefore likely to have clinical effects. We identified 156 other high-confidence heterozygous non-synonymous coding or splice variants of *IRF4* (Figure 2-source data 1) in public (gnomAD: 153 variants, all with MAF<0.009) and HGID (3 variants) databases: 147 were missense variants (two of which were also found in the homozygous state: p.S149N and p.A370V), four were frameshift indels leading to premature stop codons (p.W27YfsTer50, p.W74GfsTer28, p.Y152LeufsTer60, and S160RfsTer11), three were in-frame indels (p.E46del, p.G279_H280del, and S435del), one was a nonsense variant (p.R82*), one was an essential splice variant (c.403+2T>C), and two were missense variants found only in a non-canonical transcript predicted to undergo nonsense-mediated decay (p.L406P and p.R407W). Up to 150 of the 156 variants are predicted to be benign, whereas only six were predicted to be potentially loss-of-function (LOF) according to the gnomAD database classification (the four frameshift indels, the nonsense variant, and the essential splice variant). Comparison of the CADD score and MAF of these *IRF4* variants showed R98W to have the second highest CADD score of the four variants with a MAF < 4 $x10^{-6}$ (Figure 2). These findings suggest that the private heterozygous *IRF4* variant of this kindred is biochemically deleterious, unlike most other rare (MAF<0.009) non-synonymous variants in the general population, 150 of 156 of which were predicted to be benign (Lek et al., 2016).

R98W is loss-of-function, unlike most other previously observed IRF4 variants

We first characterized IRF4 R98W production and function *in vitro*, in an overexpression system. We assessed the effect of the *IRF4* R98W mutation on IRF4 levels by

transiently expressing WT or mutant R98W in HEK293T cells. IRF4 R98A-C99A, which is LOF for DNA binding (Brass et al., 1999), was included as a negative control. In total cell extracts, mutant IRF4 proteins were more abundant than the WT protein, and had the expected molecular weight (MW) of 51 kDa, as shown by western blotting (Figure 3A). The R98 residue has been shown to be located in a nuclear localization signal, the complete disruption of which results in a loss of IRF4 retention in the nucleus (Lau et al., 2000). We therefore analyzed the subcellular distribution of IRF4 WT and R98W proteins, in total, cytoplasmic, and nuclear extracts from transiently transfected HEK293T cells. The R98W mutant was more abundant than the WT protein in total cell and cytoplasmic extracts, but these proteins were similarly abundant in nuclear extracts (Figure 3B). We performed luciferase reporter assays to assess the ability of the mutant IRF4 protein to induce transcription from interferon-stimulated response element (*ISRE*) motif-containing promoters. Unlike the WT protein, both R98W and R98A-C99A failed to activate the $(ISRE)_3$ promoter (Figure 3C). We also assessed the ability of IRF4 to induce transcription from an (AP-1)-IRF composite element (*AICE*) motif-containing promoter (Li et al., 2012). Both R98W and R98A-C99A failed to activate the *AICE* promoter, WT protein (Figure 3D). Moreover, we observed no dominant-negative effect of the IRF4 R98W protein, with either the *ISRE* or *AICE* motif-containing promoter (Figure 3-figure supplement 1A, 1B). We assessed the ability of R98W to bind DNA, in an electrophoretic mobility shift assay (EMSA) (Figure 3E, 3F). Signal specificity was assessed by analyzing both supershift with an IRF4-specific antibody and by competition with an unlabeled competitor probe. The R98W mutation abolished IRF4 binding to the *ISRE cis* element (Figure 3E), and binding of the IRF4-PU.1 complex to interferon composite elements (EICEs) containing both IRF4 and PU.1 recognition motifs (Brass et al., 1999) (Figure 3F). The R98W allele of *IRF4* is therefore LOF for both DNA binding and the induction of transcription. We then tested 153 of the other 156

IRF4 variants: 150 variants previously described in the gnomAD database and three variants found in the HGID database. The essential splice variant and the two variants present only in a non-canonical transcript were not tested. All the variants tested were normally expressed (two with a higher MW), except for the five predicted LOF variants tested (the epitope of the antibody being at the C-terminus of IRF4) (Figure 3-figure supplement 2, 3). Transfection with the five predicted LOF plasmids was efficient, as assessed by cDNA amplification and sequencing (data not shown). When tested for $(ISRE)_3$ promoter activation, the five stop-gain or frameshift variants predicted to be LOF in the gnomAD database (very rare variants, MAF< $6x10^{-6}$) were found to be LOF. We also showed that amongall the non-synonymous coding variants tested, only one rare very rare (MAF $9x10^{-6}$) inframe deletion of one amino acid (E46del) reported in the gnomAD database, was hypomorphic, and another variant from our in-house WES database (G279_H280 del, private to one family) was LOF (Figure 3-figure supplement 4, 5). The cumulative frequency of these seven LOF (n=6) or hypomorphic (n=1) variants was $<4x10^{-5}$, fully consistent with the frequency of WD (occurring only in adults chronically infected with Tw). Overall, our data show that the R98W *IRF4* allele is LOF, like only six other very rare non-synonymous *IRF4* coding variants of the 153 variants tested. Moreover, R98W is not dominant negative.

AD IRF4 deficiency phenotypes in heterozygous EBV-B cells

We investigated the cellular phenotype of heterozygosity for the R98W allele in EBV-transformed B-cell lines (EBV-B cells) from patients. We performed reverse transcription-quantitative polymerase chain reaction (RT-qPCR) on EBV-B cells from P1, P3, two healthy heterozygous relatives (*IRF4* WT/R98W), four healthy *IRF4*-WT homozygous relatives, and seven healthy unrelated controls. We also investigated 25 unrelated WD patients with Tw

carriage. We sequenced all *IRF4* coding exons for these patients, who were found to be WT. They were also found to have an intact *IRF4* cDNA structure and normal IRF4 protein levels in EBV-B cells (data not shown). Cells from individuals heterozygous for the R98W mutation (patients and healthy carriers) had higher *IRF4* mRNA levels than those from WT homozygous relatives, unrelated WD cohort patients and EBV-B cells from healthy unrelated controls (Figure 4A). We compared the relative abundances of WT and R98W *IRF4* mRNA in EBV-B cells from heterozygous carriers of the mutation, by performing TA-cloning experiments on P1, P3, one healthy heterozygous relative, one relative homozygous for WT *IRF4*, and two previously tested healthy unrelated controls. In heterozygous carriers of the mutation (patients and healthy relatives) the R98W mutation was present in 48.1%-60% of the total *IRF4* mRNA, whereas the rest was WT (Figure 4B). We evaluated the levels and distribution of IRF4 protein by western blotting on EBV-B cells from P1, P2, P3, one healthy heterozygous relative, three healthy homozygous WT relatives and five unrelated healthy individuals. As in transfected HEK293T cells, IRF4 protein levels were high both in total cell extract and even more so in cytoplasmic extracts of EBV-B cells from heterozygous carriers (Figure 4-figure supplement 1A, 1B). By contrast, IRF4 protein levels in EBV-B cell nuclei were similar in heterozygous carriers and controls (Figure 4-figure supplement 1C). As IRF4 is a transcription factor, we then analyzed the steady-state transcriptome of EBV-B cells from three healthy homozygous WT relatives and three WT/R98W heterozygotes (P1, P3, VI.6). We identified 37 protein-coding genes as differentially expressed between subjects heterozygous for *IRF4* and those homozygous WT for *IRF4* (18 upregulated and 19 downregulated; data not shown). We identified no marked pathway enrichment based on these genes. EBV-B cells from individuals heterozygous for *IRF4* had a detectable phenotype, in terms of IRF4 production and function, consistent with AD IRF4 deficiency underlying WD.

AD IRF4 deficiency phenotypes in heterozygous leukocytes

We assessed IRF4 levels in peripheral mononuclear blood cells (PBMCs) from healthy controls (Figure 5-figure supplement 1). IRF4 were also expressed in $CD4^+$ T cells, particularly after stimulation with activating anti-CD2/CD3/CD28 monoclonal antibody-coated (mAb-coated) beads (data not shown) We therefore assessed the IRF4 protein expression profile in $CD4^+$ T cells from four healthy unrelated controls, P1 and P3, with and without (non-stimulated, NS) stimulation with activating anti-CD2/CD3/CD28 mAb-coated beads. The results were consistent with those for transfected HEK293T and EBV-B cells, as IRF4 levels were higher in activated $CD4^+$ T cells from P1 and P3 than in controls, both for total cell extracts, and even more so for the cytoplasmic compartment (Figure 5A, 5B). By contrast, IRF4 levels in the nucleus were similar and, possibly, even slightly lower in patients than in controls (Figure 5C). We also investigated peripheral myeloid (Figure 5-figure supplement 1-4) and lymphoid blood cell subsets in patients (Figure 5-figure supplement 5-7; Figure 5-data source 1) which display an apparently normal development compared to healthy controls' cells. Then,we checked for transcriptomic differences associated with genotype and/or infection, by investigating the transcriptomes of PBMCsfrom six *IRF4*-heterozygous individuals (three patients, P1-P3; and three healthy relatives, HET1-HET3) and six *IRF4* WT-homozygous individuals (four healthy relatives, WT1-WT4; and two healthy unrelated controls, C1-C2) with and without *in vitro* infection with Tw, or *Mycobacterium bovis*-Bacillus Calmette-Guerin (BCG), which, like Tw, belongs to phylum Actinobacteria, for 24 hours. We performed unsupervised hierarchical clustering of the differentially expressed (DE) transcripts (infected versus uninfected) to analyze the overall responsiveness of PBMCs from individual subjects to BCG and Tw infections *in vitro.* Heterozygous individuals clearly clustered separately from homozygous WT individuals (Figure 6A), revealing a correlation between genotype and response to infection. Overall, we found that 402 transcripts from 193

unique genes were responsive to BCG infection (Figure 6-source data 1), and 119 transcripts from 29 unique genes were responsive to Tw infection (Figure 6-source data 2) in homozygous WT subjects, according to the criteria described in the materials and methods. Due to the small number of Tw-responsive transcripts linked to unique genes, we were unable to detect any pathway enrichment for this specific condition. However, we identified 24 canonical pathways as enriched after the exposure of PBMCs to BCG. We ranked these pathways according to the difference in mean *z*-score between homozygous WT and heterozygous subjects (Figure 6B). The top 10 pathways included the interferon signaling network, the Th1 pathway network, the HMGB1 signaling network, the p38 MAPK signaling network, the NF-κB signaling network, the dendritic cell maturation network and the network responsible for producing nitric oxide and reactive oxygen species. These pathways were highly ranked mostly due to *IFNG* and *STAT1,* which were strongly downregulated in *IRF4* heterozygotes, particularly in P1, P2 and P3, relative to WT homozygotes. IRF4 is predicted to bind the promoter regions of 47% of the genes identified in the BCG study (91 of 193 genes), including those of *IFNG* and *STAT1*. Subjects heterozygous for *IRF4* also had lower levels of *LTA* expression, and lower levels of *IL2RA* expression were observed specifically in patients (GSE102862). These data suggest a general impairment of the T-cell response in subjects heterozygous for *IRF4* upon BCG infection *in vitro*. Moreover, the lower levels of *CD80* expression suggest a possible impairment of myeloid and/or antigen-presenting cell function upon BCG infection in patients, but not in healthy heterozygous or homozygous WT subjects (GSE102862). Peripheral leukocytes from *IRF4*-heterozygous individuals therefore had a phenotype in terms of IRF4 production and function.

Discussion

WD was initially described as an inflammatory disease (Whipple, 1907), but was subsequently shown to be infectious (Raoult et al., 2000; Relman et al., 1992; Yardley and Hendrix, 1961). We provide evidence that WD is also a genetic disorder. We show here that, in a large multiplex kindred, heterozygosity for the private, loss-of-function R98W mutation of *IRF4* underlies an AD form of WD with incomplete penetrance. The causal relationship between *IRF4* genotype and WD was demonstrated as follows. First, the *IRF4* R98W mutation is the only non-synonymous rare variant segregating with WD in this kindred. Second, the mutation was demonstrated experimentally to be LOF, unlike 146 of 153 other non-synonymous coding *IRF4* variants in the general population. Only seven of the 153 non-synonymous coding variants identified (including the five predicted to be LOF in the gnomAD database) were found to be LOF (n=6) or hypomorphic (n=1) and they were all extremely rare (cumulative MAF $<4x10^{-5}$). Moreover, *IRF4* has evolved under purifying selection, suggesting that deleterious heterozygous variants of this gene entail fitness costs (Barreiro and Quintana-Murci, 2010; Quintana-Murci and Clark, 2013; Rieux-Laucat and Casanova, 2014). Third, EBV-B cells and activated $CD4^+$ T cells heterozygous for *IRF4* R98W have a distinctive phenotype, particularly for IRF4 expression in the cytoplasm. This mutation also has a strong functional impact on gene expression in *IRF4* R98W-heterozygous PBMCs stimulated with BCG or Tw. These findings unequivocally show that heterozygosity for the R98W allele of *IRF4* is the genetic etiology of WD in this kindred. Although we did not find any *IRF4* mutations in a pilot cohort of 25 patients with sporadic WD, these and other patients may also develop WD due to other inborn errors of immunity, possibly related to IRF4, as suggested by the apparent genetic heterogeneity and physiological homogeneity underlying severe infectious diseases (Casanova, 2015a; Casanova, 2015b). This observation therefore extends our model, in which life-threatening infectious diseases striking otherwise

healthy individuals during primary infection can result from single-gene inborn errors of immunity.

In this kindred with AD IRF4 deficiency, haploinsufficiency was identified as the key mechanism, although IRF4 protein levels in the cytoplasmic compartment were higher in patients with the mutation than in wild-type homozygotes. The protein was not more abundant in the nucleus, where IRF4 exerts its effects on transcription. Moreover, half of the *IRF4* mRNA in EBV-B cells from heterozygous subjects is WT. The total amount of *IRF4* mRNA was higher in the EBV-B cells of heterozygous subjects, but the total amount of IRF4 protein in the nuclear compartment of heterozygous EBV-B and activated $CD4^+$ T cells was similar to that in WT homozygous cells. These data suggest that no more than half the IRF4 protein in the nucleus is WT in heterozygous cells. In addition, not only is *IRF4* subject to purifying selection, but the R98W mutation is itself LOF, with no detectable dominant-negative effect at cell level. Haploinsufficiency is an increasingly recognized mechanism underlying AD inborn errors of immunity (Afzali et al., 2017; Rieux-Laucat and Casanova, 2014). It is commonly due to loss-of-expression alleles, contrasting with the negative dominance typically exerted by expressed proteins, but many mutations are known to cause haploinsufficiency without actually preventing protein production (Afzali et al., 2017; Perez de Diego et al., 2010; Rieux-Laucat and Casanova, 2014). Haploinsufficiency in this kindred is not due to loss of expression of IRF4. Instead, it results from a lack of activity of the R98W IRF4 proteins present in the nucleus.

Incomplete penetrance is common in conditions resulting from haploinsufficiency. In this kindred, incomplete penetrance may result from a lack of Tw infection (in heterozygous individuals IV.5 and VI.7), or a lack of WD development in infected individuals (in heterozygous individuals III.6, IV.4, V.3, V.4, VI.6). All five chronic carriers of Tw were heterozygous for the *IRF4* R98W mutation, suggesting that AD IRF4 deficiency also favors

the development of chronic Tw carriage. The five asymptomatic carriers were 24 to 82 years old, whereas the four patients were 69 to 92 years old. The impact of IRF4 R98W may therefore increase with age, initially facilitating chronic carriage in Tw-infected individuals, and subsequently predisposing chronic carriers to the development of WD. We cannot exclude the possibility that a modifier allele at another locus contributes to the development of WD in infected heterozygous individuals with *IRF4* mutations. Future studies will attempt to define the cellular basis of WD in individuals with *IRF4* mutations. The apparently normal development of all peripheral myeloid and lymphoid blood cell subsets studied in patients, and the selective predisposition of these individuals to WD suggest that the disease mechanism is subtle and specifically affects protective immunity to Tw, and that it may act in the gastrointestinal (GI) tract. Interestingly, the data of several public databases indicate that *IRF4* RNA is expressed in the stomach, colon, and small intestine (https://www.gtexportal.org, http://biogps), and that the IRF4 protein is expressed in glandular cells from the stomach, duodenum, small intestine, and rectum (https://www.proteinatlas.org). In addition, a recent analysis of human intestinal macrophage subsets (Bujko et al., 2017) showed *IRF4* RNA to be expressed in human intestinal myeloid resident cells. Further studies of GI tract-resident cells, including myeloid and lymphoid cells in particular, should make it possible to decipher the molecular and cellular mechanisms by which human IRF4 haploinsufficiency underlies WD upon infection by Tw.

Materials and Methods

Patients and family

All members of the multiplex kindred studied, the pedigree of which is shown in Figure 1A, live in France and are of French descent. Informed consent was obtained from all family members, and the study was approved by the national ethics committee.

Patient 1 (P1, proband) was born in 1948 and presented arthritis of the right knee in 2011, after recurrent episodes of arthritis of this joint associated with effusion since 1980. *Tropheryma whipplei* (Tw) was detected in synovial fluid by PCR and culture in 2011, but was not detected by PCR in saliva, feces, and small-bowel biopsy specimens. Physical examination revealed a large effusion of the right knee, limiting mobility. The fluid aspirated from this joint contained 4,000 erythrocytes/mm^3 and 8,800 leukocytes/mm^3, but no crystals or evidence of microbes. Synovial hypertrophy of the right knee and a narrowing of the right internal femoro-tibial joint were detected on MRI. X ray showed an extension of the right femoro-tibial joint and erosion of the posterior part of the femoro-tibial joint. However, erythrocyte sedimentation rate (ESR) (3 mm/h) and C-reactive protein (CRP) (1.8 mg/l) determinations gave negative results. P1 received methotrexate (15 mg/week) for four months, without remission. Antibiotic treatment with doxycycline (200 mg/day) was then immediately initiated. The arthralgia resolved, but right knee effusion persisted. Hydroxychloroquine was therefore added to the treatment regimen. At last follow-up, in 2016, the patient was well.

P2, a second cousin of P1, was born in 1941 and was diagnosed with classical WD and digestive problems in 1978, based on positive periodic acid–Schiff (PAS) staining of a small intestine biopsy specimen. She was treated with sulfamethoxazole/trimethoprim. At last follow-up, in 2016, Tw PCR was positive for the saliva and feces.

P3, the father of P1, was born in 1925 and was diagnosed with classical WD in 1987 on the basis of positive PAS staining of a small intestine biopsy specimen. Clinical manifestations included diarrhea, abdominal pain and weight loss. P3 displayed no extraintestinal manifestations. He was successfully treated with sulfamethoxazole/trimethoprim, with complete clinical and bacteriological remission.

P4, the brother of P2, was born in 1947 and sought medical advice in 2015 for arthralgia affecting the knees and right ulna-carpal joints. The other joints were unaffected. A culture of the joint fluid was negative for bacteria, but Tw was not sought. Tw was not detected in the saliva and feces by PCR or culture, but serological tests for Tw were positive. P4 had no rheumatoid factor, anti-cyclic citrullinated peptide antibodies (anti-CCP), or anti-nuclear antibodies. The fluid aspirated from the right knee contained 4,800 erythrocytes/mm^3 and 10,900 leukocytes/mm^3 (91% neutrophils and 9% lymphocytes) without crystals. Blood tests revealed an ESR of 30 mm/h and a CRP concentration of 50 mg/l, with no rheumatoid factor, anti-cyclic citrullinated peptide antibodies (anti-CCP) or anti-nuclear antibodies. An X ray revealed a narrowing of the joint space in the knees and vertebral hyperostosis was visible. The joints of the hands were unaffected. The patient was treated with anti-inflammatory drugs, without success. Treatment with methotrexate and steroids was introduced, followed by antibiotics, the effect of which is currently being evaluated.

Saliva and/or feces samples from 18 other members of the family were checked for the presence of Tw, by a PCR specifically targeting *T. whipplei*, as previously described (Figure 1A, table 1) (Edouard et al., 2012). Five individuals were found to be chronic carriers (mean age: 55 years) and 13 were not (mean age: 38 years). Testing was not possible for nine other relatives. The overall distribution of WD in this kindred was suggestive of an AD trait with incomplete penetrance.Genome-wide analysis

Genome-wide linkage analysis was performed by combining genome-wide array and whole-exome sequencing (WES) data (Belkadi et al., 2016). In total, nine family members were genotyped with the Genome-Wide Human SNP Array 6.0. Genotype calling was achieved with the Affymetrix Power Tools Software Package (http://www.affymetrix.com/estore/partners_programs/programs/developer/tools/powertools.affx). SNPs were selected with population-based filters (Purcell et al., 2007), resulting in the use of 905,420 SNPs for linkage analysis. WES was performed as described in the corresponding section, in four family members, P1, P2, P3 and P4. In total, 64,348 WES variants were retained after application of the following filtering criteria: genotype quality (GQ) > 40, minor read ratio (MRR) > 0.3, individual depth (DP) > 20x, retaining only diallelic variants with an existing RS number and a call rate of 100%. Parametric multipoint linkage analysis was performed with the Merlin program (Abecasis et al., 2002), using the combined set of 960,267 variants. We assumed an AD mode of inheritance, with a frequency of the deleterious allele of 10^{-5} and a penetrance varying with age (0.8 above the age of 65 years, and 0.02 below this threshold). Data for the family and for Europeans from the 1000G project were used to estimate allele frequencies and to define linkage clusters, with an r^2 threshold of 0.4.

The method used for WES has been described elsewhere (Bogunovic et al., 2012; Byun et al., 2010). Briefly, genomic DNA extracted from the patients' blood cells was

sheared with a Covaris S2 Ultrasonicator (Covaris). An adapter-ligated library was prepared with the Paired-End Sample Prep kit V1 (Illumina). Exome capture was performed with the SureSelect Human All Exon kit (71 Mb version - Agilent Technologies). Paired-end sequencing was performed on an Illumina Genome Analyzer IIx (Illumina), generating 72- or 100-base reads. We used a BWA-MEM aligner (Li and Durbin, 2009) to align the sequences with the human genome reference sequence (hg19 build). Downstream processing was carried out with the Genome analysis toolkit (GATK) (McKenna et al., 2010) SAMtools (Li et al., 2009), and Picard Tools (http://picard.sourceforge.net). Substitution calls were made with a GATK UnifiedGenotyper, whereas indel calls were made with a SomaticIndelDetectorV2. All calls with a read coverage <2x and a Phredscaled SNP quality <20 were filtered out. Single-nucleotide variants (SNV) were filtered on the basis of dbSNP135 (http://www.ncbi.nlm.nih.gov/SNP/) and 1000 Genomes (http:browser.1000genomes.org/index.html) data. All variants were annotated with ANNOVAR (Wang et al., 2010). All *IRF4* mutations identified by WES were confirmed by Sanger sequencing.

Tw detection

PCR and serological tests for Tw were performed as previously described (Fenollar et al., 2009).

Cell culture and subpopulation separation

PBMCs were isolated by Ficoll-Hypaque density centrifugation (GE Healthcare) from cytopheresis or whole-blood samples obtained from healthy volunteers and patients,

respectively. PBMCs and EBV-B cells (B-cell lines homemade transformed with EBV) were cultured in RPMI medium supplemented with 10% FBS, whereas HEK293T cells (ATCC; CRL-3216) were cultured in DMEM medium supplemented with 10% FBS. Subsets were separated by MACS, using magnetic beads conjugated with the appropriate antibody (Miltenyi Biotec) according to the manufacturer's protocol. All cells used in this study were tested for mycoplasma contamination and found to be negative.

Site-directed mutagenesis and transient transfection

The full-length cDNA of *IRF4* and *PU.1* was inserted into the pcDNA™ 3.1D/V5-His-TOPO® vector with the directional TOPO expression kit (Thermo Fisher Scientific). *BATF anf JUN* were obtained from Origene companie (#RC207104 and #RC209804 respectively). Constructs carrying mutant alleles were generated from this plasmid by mutagenesis with a site-directed mutagenesis kit (QuikChangeII XL; Agilent Technologies), according to the manufacturer's instructions. HEK293T cells were transiently transfected with the various constructs, using the Lipofectamine LTX kit (Thermo Fisher Scientific) in accordance with the manufacturer's instructions.

Cell lysis and western blotting

Total protein extracts were prepared by mixing cells with lysis buffer (50 mM Tris-HCl pH 7.4, 150 mM NaCl, 0.5% Triton X-100, and 2 mM EDTA) supplemented with protease inhibitors (Complete, Roche) and phosphatase inhibitor cocktail (PhoStop, Roche), 0.1 mM dithiothreitol DTT (Life Technologies), 10 µg/ml pepstatin A (Sigma, #P4265), 10 µg/ml leupeptin (Sigma, #L2884), 10 µg/ml antipain dihydrochloride (Sigma, #A6191) and incubating for 40 minutes on ice. A two-step extraction was performed to separate the

cytoplasmic and nuclear content of the cells; cells were first mixed with a membrane lysis buffer (10 mM Hepes pH 7.9, 10 mM KCl, 0.1 mM EDTA, 0.1 mM EGTA, 0.05 % NP40, 25 mM NaF supplemented with 1 mM PMSF, 1 mM DTT, 10 µg/ml leupeptin, 10 µg/ml aprotinin) and incubated for 30 minutes on ice. The lysate was centrifuged at 10,000 x *g*. The supernatant, corresponding to the cytoplasm-enriched fraction, was collected and the nuclear pellet was mixed with nuclear lysis buffer (20 mM Hepes pH 7.9, 0.4 M NaCl, 1,mM EDTA, 1, mM EGTA, 25% glycerol supplemented with 1 mM PMSF, 1 mM DTT, 10 µg/ml leupeptin, 10 µg/ml aprotinin). Equal amounts of protein, according to a Bradford protein assay (BioRad, Hercules, California, USA), were resolved by SDS-PAGE in a Criterion™ TGX™ 10% precast gel (Biorad) and transferred to a low-fluorescence PVDF membrane. Membranes were probed with unconjugated antibody: anti-IRF4 (Santa Cruz, M-17) antibody was used at a dilution of 1:1000 and antibodies against GAPDH (Santa Cruz, FL-335), topoisomerase I (Santa Cruz, C-21), and/or lamin A/C (Santa Cruz, H-110) were used as loading controls. The appropriate HRP-conjugated or infrared dye (IRDye)-conjugated secondary antibodies were incubated with the membrane for the detection of antibody binding by the ChemiDoc MP (Biorad) or Licor Odyssey CLx system (Li-Cor, Lincoln, Nebraska, USA) respectively.

EMSA

Double-stranded unlabeled oligonucleotides (cold probes) were generated by annealing in TE buffer (pH 7.9) supplemented with 33.3 mM NaCl and 0.67 mM $MgCl_2$. The annealing conditions were 100°C for 5 minutes, followed by cooling overnight at room temperature. After centrifugation at 3,000 x *g* at 4°C for 30 minutes, the pellet was suspended in water. We labeled 0.1 µg of cold probe in Klenow buffer supplemented with 9.99 mM

dNTP without ATP, 10 U Klenow fragment (NEB) and 50 µCi d-ATP-^{32}P, at 37°C for 60 minutes. Labeled probes were purified on Illustra MicroSpin G-25 Columns (GE Healthcare Life Sciences), according to the manufacturer's protocol. We incubated 10 µg of nuclear protein lysate on ice for 30 minutes with a ^{32}P-labeled (a-dATP) *ISRE* probe (5' – gat cGG GAA AGG GAA ACC GAA ACT GAA-3') designed on the basis of the *ISG15* promoter or the λB probe (5'- gat cGC TCT TTA TTT TCC TTC ACT TTG GTT AC-3') described by Brass et al. in 1999 (Brass et al., 1999). For supershift assays, nuclear protein lysates were incubated for 30 minutes on ice with 2 µg of anti-IRF4 (Santa Cruz, M-17) antibody or anti-goat Ig (Santa Cruz) antibody. Protein/oligonucleotide mixtures were then subjected to electrophoresis in 12.5% acrylamide/bis-acrylamide 37.5:1 gels in 0.5% TBE migration buffer for 80 minutes at 200 mA. Gels were dried on Whatman paper at 80°C for 30 minutes and placed in a phosphor-screen cassette for five days. Radioactivity levels were analyzed with the Fluorescent Image Analyzer FLA-3000 system (Fujifilm).

Luciferase reporter assays

The $(ISRE)_3$ reporter plasmid (pGL4.10[luc2] backbone, Promega #E6651), which contains three repeats of the *ISRE* sequence separated by spacers, was kindly provided by Prof. Aviva Azriel (Department of Biotechnology and Food Engineering, Technion-Israel Institute of Technology). The *AICE* reporter plasmid (pGL4.10[luc2] backbone, Promega #E6651) contains part of the *IL23R* promoter (-254 to -216). HEK293T cells were transiently transfected with the $(ISRE)_3$ reporter plasmid (100 ng/well on a 96-well plate), the pRL-SV40 vector (Promega # E2231, 40 ng/well) and a *IRF4* WT or mutant pcDNA™ 3.1D/V5-His-TOPO® plasmid (Invitrogen #K4900-01, 25 ng/well or the amount indicated, made up to 100 ng with empty plasmid), with the Lipofectamine LTX kit (Thermo Fisher Scientific), according to the manufacturer's instructions. For the *AICE* assay, we used the same protocol,

but with the addition of *BATF* and *JUN* expression plasmids (25 ng/well each). Cells were used 24 h after transfection for the *ISRE* assay and 48 h after transfection for the *AICE* assay, with the Dual-Luciferase® 1000 assay system kit (Promega #E1980), according to the manufacturer's protocol. Signal intensity was determined with a Victor™ X4 plate reader (Perkin Elmer). Experiments were performed in triplicate and reporter activity is expressed as fold-induction relative to cells transfected with the empty vector. Negative dominance was assessed by performing the same protocol with the following modifications: $(ISRE)_3$ reporter plasmid (100 ng/well for a 96-well plate), pRL-SV40 vector (40 ng/well) WT and mutant plasmids were used to cotransfect cells, with a constant amount of WT plasmid (25 ng/well) but various amounts of mutant plasmid (25 ng/well alone made up to 100 ng with empty plasmid or with the indicated amount, made up to 100 ng with empty plasmid) amounting to a total of 240 ng/well. For the *AICE* assay, the same protocol was used, but with the addition of *BATF* and *JUN* expression plasmids (25 ng/well each).

Microarrays

For the microarray analysis of PBMCs, cells from six *IRF4*-heterozygous individuals (three patients, P1-P3; and three asymptomatic relatives, HET1-HET3) and six *IRF4* WT-homozygous individuals (four healthy relatives, WT1-WT4; and two healthy unrelated controls, C1-C2) were dispensed into a 96-well plate at a density of 200,000 cells/well and were infected *in vitro* with live Tw at a multiplicity of infection (MOI) of 1, or with live BCG (*M. bovis*-BCG, Pasteur substrain) at a MOI of 20, or were left uninfected (mock). Two wells per condition were combined 24 h post-infection for total RNA isolation with the ZR RNA Microprep™ kit (Zymo Research). For the microarray on EBV-B cells, we used 400,000 cells from three *IRF4*-heterozygous mutation carriers and three WT individuals from the kindred for total RNA isolation with the ZR RNA Microprep™ kit (Zymo Research). Microarray

589 experiments on both PBMCs and EBV-B cells were performed with the Affymetrix Human
590 Gene 2.0 ST Array. Raw expression data were normalized by the robust multi-array average
591 expression (RMA) method implemented in the affy R package (Gautier et al., 2004; Irizarry et
592 al., 2003). Normalized expression data were processed as previously described (Alsina et al.,
593 2014) and briefly summarized here. First, fold-changes (FC) in expression between mock-
594 infected and BCG-infected or Tw-infected conditions were calculated for each individual
595 separately. For each set of conditions, transcripts were further filtered based on a minimal 1.5
596 FC in expression (up- or downregulation). In a final stage, transcripts satisfying the previous
597 filters in at least four of the six homozygous WT individuals for each *in vitro* infection
598 condition were retained for downstream analysis. We counted the differentially expressed
599 (DE) transcripts affected by stimulation in samples from all subjects for each stimulus, and
600 determined the mean counts for these DE transcripts in all homozygotes. The mean values
601 obtained were then used to normalize the counts of DE transcripts, yielding an overall
602 transcriptional responsiveness for each individual separately, and for each stimulus. This
603 overall responsiveness of subjects to either Tw or BCG is shown as a heatmap, and individual
604 subjects were grouped by unsupervised hierarchical clustering. Responsive transcripts were
605 further analyzed with Ingenuity Pathway Analysis (IPA) Software, Version 28820210
606 (QIAGEN) (Alsina et al., 2014) for functional interpretation. In brief, the FC values for each
607 individual and treatment were used as input data for the identification of canonical pathway
608 enrichment (*z*-score cut-off set at 0.1). The activation *z*-score values calculated for the
609 identified pathways were exported from IPA and used to calculate mean values and
610 differences between WT homozygotes and heterozygotes, and for graphical representation,
611 with Microsoft Excel and GraphPad Prism Version 7.0, respectively. The direction of the
612 difference was not considered further. Negative mean difference values were converted into
613 positive values before the ranking of the canonical pathways according to the difference

between the genotypes. The microarray data used in this study have been deposited in the NCBI Gene Expression Omnibus (GEO) database, under accession number GSE102862.

IRF4 qPCR

Total RNA was prepared from the EBV-B cells of individuals heterozygous for *IRF4* mutations (two patients and two asymptomatic relatives), and healthy homozygous WT relatives (*n*=4). We also included samples from unrelated individuals (seven healthy controls and 25 patients with Tw carriage; all *IRF4* coding exons for each individual were sequenced and shown to be WT). Moreover, the 25 WD patients included in this experiment were found to have an intact *IRF4* cDNA structure and normal levels of IRF4 protein production in EBV-B cells. RNA was prepared from 500,000 cells with the ZR RNA Microprep™ kit (Zymo Research), according to the manufacturer's instructions. A mixture of random octamers and oligo dT-16 was used, with the MuLV reverse transcriptase (High-Capacity RNA-to-cDNA™ kit, Thermo Fisher Scientific), to generate cDNA. Quantitative real-time PCR was performed with the TaqMan® Universal PCR Master Mix (Thermo Fisher Scientific), the *IRF4*-specific primer (Hs01056533_m1, Thermo Fisher Scientific) and the endogenous human β-glucuronidase (*GUSB*) as a control (4326320E, Thermo Fisher Scientific). Data were analyzed by the ΔΔCt method, with normalization against *GUSB*.

IRF4 TA-cloning

The full-length cDNA generated from the EBV-B cells of *IRF4*-heterozygous and WT homozygous individuals was used for the PCR amplification of exon 3 of *IRF4*. The products obtained were cloned with the TOPO TA cloning kit (pCR2.1®-TOPO® TA vector, Thermo Fisher Scientific), according to the manufacturer's instructions. They were then used to

transform chemically competent bacteria, and 100 clones per individual were Sanger-sequenced with M13 primers (forward and reverse).

$CD4^+$ T-cell stimulation by activating anti-CD2/CD3/CD28 mAb-coated beads

Isolated $CD4^+$ T cells from patients (P1 and P3) and from healthy unrelated controls (C1-C4) were either left unstimulated (NS) or stimulated with activating anti-CD2/CD3/CD28 mAb-coated beads (Miltenyi Biotec) for 24 h in RPMI medium supplemented with 10% FBS (24-well plate).

Differentiation and activation of *in vitro* monocyte-derived macrophages (MDMs)

After isolation, monocytes from P1 or two healthy unrelated controls were plated (24-well plate; 600,000 cells/well) in RPMI medium supplemented with 40% human serum (M1-like) or 10% FBS (M2-like). Differentiation cytokines (R&D Systems) were immediately added: 0.5 ng/ml rhGM-CSF (M1-like) or 20 ng/ml rhM-CSF (M2-like). Every three days, we replaced 30% of the medium with fresh complete medium supplemented with the appropriate cytokines. After 14 days of differentiation, cells were left unstimulated (NS) or were activated by incubation with 2.5 ng/ml IFN-γ (M1-like) or 50 ng/ml rh-IL-4 (M2-like) for 48 h.

MDM surface marker expression

Differentiated/activated MDMs were detached by treatment with trypsin (1.6 µg/ml) in PBS. Cells were treated with Fc receptor blocking agent (Miltenyi Biotec) and Aqua Dead Cell Stain kit (Thermo Fisher Scientific) for 1 h. They were then washed and stained for 1 h at room temperature with appropriate antibodies (see Figure 5-figure supplement 4) and

appropriate isotype controls (BD biosciences). Samples were analyzed on a Beckman Coulter Gallios flow cytometer.

Percentage of memory B cells

PBMCs from healthy unrelated controls and patients (P1, P2 and P3) were stained with antibodies against CD20, CD10 and CD27, and IgM, IgD, IgG or IgA. The percentages of transitional ($CD20^+$ $CD10^+$ $CD27^-$), naïve ($CD20^+$ $CD10^-$ $CD27^-$) and memory ($CD20^+$ $CD10^-$ $CD27^+$) B cells were determined by flow cytometry. We then assessed the IgM/IgD or IgG or IgA expression of the memory B cells, to determine the extent of Ig isotype switching in the memory compartment.

Ex vivo naïve and effector/memory $CD4^+$ T-cell stimulation

$CD4^+$ T cells were isolated as previously described (Ma et al., 2012). Briefly, cells were labeled with anti-CD4, anti-CD45RA, and anti-CCR7 antibodies, and naïve (defined as $CD45RA^+$ $CCR7^+$ $CD4^+$) T cells or effector/memory T cells (defined as $CD45RA^-CCR7^{\pm}$ $CD4^+$) were isolated (> 98% purity) with a FACS Aria cell sorter (BD Biosciences). Purified naïve or effector/memory $CD4^+$ T cells were cultured with T-cell activation and expansion beads (anti-CD2/CD3/CD28; Miltenyi Biotec) for five days. Culture supernatants were then used to assess the secretion of IL-2, IL-4, IL-5, IL-6, IL-9, IL-10, IL-13, IL-17A, IL-17F, IFNγ and TNFα in a cytometric bead array (BD biosciences), and the secretion of IL-22, by ELISA (Peprotech).

In vitro differentiation of naïve CD4$^+$ T cells

Naïve CD4$^+$ T cells (CD45RA$^+$CCR7$^+$) were isolated (> 98% purity) from healthy unrelated controls or patients, with a FACS Aria sorter (BD Biosciences). They were cultured under polarizing conditions, as previously described (Ma et al., 2016). Briefly, cells were cultured with T-cell activation and expansion beads (anti-CD2/CD3/CD28; Miltenyi Biotec) alone or under Th1 (IL-12 [20 ng/ml; R&D Systems]) or Th17 (TGFβ, IL-1β [20 ng/ml; Peprotech], IL-6 [50 ng/ml; PeproTech], IL-21 [50 ng/ml; PeproTech], IL-23 [20 ng/ml; eBioscience], anti-IL-4 [5 μg/ml], and anti-IFN-γ [5 μg/ml; eBioscience]) polarizing conditions. After five days, culture supernatants were used to assess the secretion of the cytokines indicated, by ELISA (IL-22), or with a cytometric bead array (all other cytokines).

Key resources table

Reagent type (species) or resource	Designation	Source or reference	Identifiers	Additional information
gene (Human)	*IRF4* (NM_002460.3)	This paper		vector backbone: pcDNA™ 3.1D/V5-His-TOPO® vector (Thermo Fisher Scientific)
gene (Human)	*PU.1* (NM_001080547.1)	This paper		vector backbone: pcDNA™ 3.1D/V5-His-TOPO® vector (Thermo Fisher Scientific)
gene (Human)	*BATF* (NM_006399.3)	OriGene	RC207104	
gene (Human)	*JUN* (NM_002228.3)	OriGene	RC209804	
strain (Tropheryma whipplei), strain background (DIG APD 25)	Tw	This paper	NCBI taxon: 2039	Obtained from "Research Unit of Infectious and Tropical Emerging Diseases, University Aix-Marseille, URMITE, UM63, CNRS 7278, IRD 198, 13005 Marseille, France, EU". Strain isolated from mesenteric lymph node (29/01/09).
strain (Mycobacterium bovis-Bacillus Calmette-Guerin), strain background (pasteur)	BCG	doi: 10.1084/jem.20021769	NCBI taxon: 33892	
cell line (Human)	HEK293T	ATCC	CRL-3216	

Reagent type (species) or resource	Designation	Source or reference	Identifiers	Additional information
cell line (Human)	EBV-B cells	This paper		For each individual, purified B cells were immortalized with EBV in the laboratory
transfected construct (PGL4.10[luc2])	(ISRE)3 reporter plasmid,	This paper, backbone: Promega	#E6651	Obtained from "Department of Biotechnology and Food Engineering, Technion-Israel Institute of Technology"
transfected construct (PGL4.10[luc2])	*AICE* reporter plasmid	This paper, backbone: Promega	#E6651	Generated by metabion international ag
transfected construct (pRL-SV40 vector)	pRL-SV40 vector	Promega	#E2231	
biological sample (Human)	Patients' blood samples	This paper		
biological sample (Human)	Controls' blood samples	This paper		
antibody	anti-IRF4	Santa Cruz	M-17	dillution: 1/1000
antibody	anti-GAPDH	Santa Cruz	FL-335	dillution: 1/1000
antibody	anti-topoisomerase I	Santa Cruz	C-21	dillution: 1/1000
antibody	anti-lamin A/C	Santa Cruz	H-110	dillution: 1/1000
antibody	anti-lamin A/C	Santa Cruz	H-110	dillution: 1/1000
antibody	anti-CD11b	Miltenyi Biotec	# 130-110-611	fluorochrome: PE
antibody	anti-CD86	Miltenyi Biotec	#130-094-877	fluorochrome: PE
antibody	anti-CD206	Miltenyi Biotec	#130-099-732	fluorochrome: PE
antibody	anti-CD209	Miltenyi Biotec	#130-109-589	fluorochrome: PE
antibody	anti-HLADR	Miltenyi Biotec	#130-111-789	fluorochrome: PE
antibody	anti-CD20	BD biosciences		fluorochrome: PE; clone H1
antibody	anti-CD10	BD biosciences		fluorochrome: APC, clone HI10a
antibody	anti-CD27	BD biosciences		fluorochrome: PerCP-Cy5.5; clone L128
antibody	anti-IgM	Miltenyi		clone PJ2-22H3
antibody	anti-IgG	BD biosciences		fluorochrome: BV605; clone G18-145
antibody	anti-IgA	Miltenyi		clone IS11-8E10
antibody	anti-CD4	eBioscience		fluorochrome: Pacific blue; clone OKT4
antibody	anti-CD45RA	BD biosciences		fluorochrome: PerCP-Cy5.5, clone HI100
antibody	anti-CCR7	Sony		fluorochrome: FITC; clone G043H7
recombinant DNA reagent	pcDNA™ 3.1D/V5-His-TOPO® vector	Thermo Fisher Scientific	#K4900-01	
sequence-based reagent	IRF4-specific primer	Thermo Fisher	#Hs01056533_m1	

Reagent type (species) or resource	Designation	Source or reference	Identifiers	Additional information
		Scientific		
sequence-based reagent	GUSB	Thermo Fisher Scientific	#4326320E	
peptide, recombinant protein	rhGM-CSF	R&D System	#CAA26822	
peptide, recombinant protein	rhM-CSF	R&D System	#NP_757350	
peptide, recombinant protein	IFN-γ	Boehringer Ingelheim		Imukin
peptide, recombinant protein	rhIL4	R&D System	#P05112	
commercial assay or kit	Lipofectamine LTX kit	Thermo Fisher Scientific	#15338100	
commercial assay or kit	Dual-Luciferase® 1000 assay system kit	Promega	#E1980	
commercial assay or kit	ZR RNA Microprep™ kit	Zymo research	#R1061	
commercial assay or kit	High-Capacity RNA-to-cDNA™ kit	Thermo Fisher Scientific	#R4387406	
commercial assay or kit	TOPO TA cloning kit	Thermo Fisher Scientific	#K450001	
commercial assay or kit	directional TOPO expression kit	Thermo Fisher Scientific	#K4900-01	
commercial assay or kit	QuikChangeII XL Site-Directed Mutagenesis Kit	Agilent Technologies	#200522	
commercial assay or kit	LIVE/DEAD™ Fixable Aqua Dead Cell Stain Kit	Thermo Fisher Scientific	#L34957	
chemical compound, drug	Tris	MP biomedicals	#11TRIS01KG	
chemical compound, drug	HCl	Sigma	#H1758	
chemical compound, drug	NaCl	Sigma	#S3014	
chemical compound, drug	Triton X-100	Sigma	#T8532	
chemical compound, drug	EDTA	MP biomedicals	#11EDTA05M1	
chemical compound, drug	protease inhibitors Complete	Roche	#04693116001	
chemical compound, drug	Phosphatase inhibitor cocktail	Roche	#04906837001	
chemical compound, drug	DTT	Thermo Fisher Scientific	#20290	

Reagent type (species) or resource	Designation	Source or reference	Identifiers	Additional information
chemical compound, drug	pepstatin A	Sigma	#P4265	
chemical compound, drug	leupeptin	Sigma	#L2884	
chemical compound, drug	antipain	Sigma	#A6191	
chemical compound, drug	Hepes	Sigma	#H3375	
chemical compound, drug	KCl	Sigma	#P9333	
chemical compound, drug	EGTA	Amresco	#0732	
chemical compound, drug	NP40	Sigma	#N6507	
chemical compound, drug	NaF	Sigma	#S7920	
chemical compound, drug	PMSF	Sigma	#P7626	
chemical compound, drug	MgCl2	Sigma	#M8266	
chemical compound, drug	Klenow fragment	NEB	#M0210S	
chemical compound, drug	d-ATP-32P	PerkinElmer	#BLU012H250UC	
chemical compound, drug	TBE migration buffer	Euromedex	#ET020-B	
chemical compound, drug	acrylamide/bis-acrylamide 37.5:1	Sigma	#A7168	
software, algorithm	affy R package	Gautier, Cope, Bolstad, & Irizarry, 2004; Irizarry et al., 2003)		
software, algorithm	IPA software	Alsina et al., 2014		
software, algorithm	Microsoft Excel	Microsoft		
software, algorithm	GraphPad Prism V7.0	GraphPad		
software, algorithm	Image studio	Licor		

694

695

Acknowledgments

We thank the patients and their families for participating in the study. We thank Yelena Nemirovskaya, Tatiana Kochetkov, Lahouari Amar, Cécile Patissier, Céline Desvallées, Dominick Papandrea, Mark Woollett, and Amy Gall for technical and secretarial assistance and all members of the Laboratory of Human Genetics of Infectious Diseases for helpful discussions. We acknowledge the use of the biological resources of the Imagine Institute DNA biobank (BB-33-00065). A.G. was supported by ANR-IFNPHOX (ANR-13-ISV3-0001-01), ANR-GENMSMD (ANR-16-CE17-0005-01) and the Imagine Institute. The Laboratory of Human Genetics of Infectious Diseases is supported in part by grants from the St. Giles Foundation, The Rockefeller University, Institut National de la Santé et de la Recherche Médicale (INSERM), Paris Descartes University, and the European Research Council (ERC), the Integrative Biology of Emerging Infectious Diseases Laboratory of Excellence (ANR-10-LABX-62-IBEID) and the French National Research Agency (ANR) under the "Investments for the future" program (grant number ANR-10-IAHU-01), ANR-IFNPHOX (ANR-13-ISV3-0001-01, to J.B.), ANR-GENMSMD (ANR-16-CE17-0005-01, to J.B.). Research in the Quintana-Murci laboratory was supported by the Pasteur Institute, the *Centre National de la Recherche Scientifique* (CNRS), the French Government's Investissement d'Avenir program, (ANR-10-LABX-62-IBEID), IEIHSEER (ANR-14-CE14-0008-02) and TBPATHGEN (ANR-14-CE14-0007-02), and the European Union's Seventh Framework Program (FP/2007–2013)/ERC Grant Agreement No. 281297. S.G.T. and C.S.M. are supported by grants and fellowship awarded by the National Health and Medical Research Council of Australia (1113904, 1042925) and the Office of Health and Medical Research of the New South Wales State Government. T.N. and L.W. are supported by Australian Postgraduate Research Awards from the University of NSW.

References

Abecasis, G.R., S.S. Cherny, W.O. Cookson, and L.R. Cardon. 2002. Merlin--rapid analysis of dense genetic maps using sparse gene flow trees. *Nat Genet* 30:97-101.

Afzali, B., J. Gronholm, J. Vandrovcova, C. O'Brien, H.W. Sun, I. Vanderleyden, F.P. Davis, A. Khoder, Y. Zhang, A.N. Hegazy, A.V. Villarino, I.W. Palmer, J. Kaufman, N.R. Watts, M. Kazemian, O. Kamenyeva, J. Keith, A. Sayed, D. Kasperaviciute, M. Mueller, J.D. Hughes, I.J. Fuss, M.F. Sadiyah, K. Montgomery-Recht, J. McElwee, N.P. Restifo, W. Strober, M.A. Linterman, P.T. Wingfield, H.H. Uhlig, R. Roychoudhuri, T.J. Aitman, P. Kelleher, M.J. Lenardo, J.J. O'Shea, N. Cooper, and A.D.J. Laurence. 2017. BACH2 immunodeficiency illustrates an association between super-enhancers and haploinsufficiency. *Nat Immunol* 18:813-823.

Alsina, L., E. Israelsson, M.C. Altman, K.K. Dang, P. Ghandil, L. Israel, H. von Bernuth, N. Baldwin, H. Qin, Z. Jin, R. Banchereau, E. Anguiano, A. Ionan, L. Abel, A. Puel, C. Picard, V. Pascual, J.L. Casanova, and D. Chaussabel. 2014. A narrow repertoire of transcriptional modules responsive to pyogenic bacteria is impaired in patients carrying loss-of-function mutations in MYD88 or IRAK4. *Nat Immunol* 15:1134-1142.

Amsler, L., P. Bauernfeind, C. Nigg, R.C. Maibach, R. Steffen, and M. Altwegg. 2003. Prevalence of Tropheryma whipplei DNA in patients with various gastrointestinal diseases and in healthy controls. *Infection* 31:81-85.

Andersen, L.L., N. Mork, L.S. Reinert, E. Kofod-Olsen, R. Narita, S.E. Jorgensen, K.A. Skipper, K. Honing, H.H. Gad, L. Ostergaard, T.F. Orntoft, V. Hornung, S.R. Paludan, J.G. Mikkelsen, T. Fujita, M. Christiansen, R. Hartmann, and T.H. Mogensen. 2015. Functional IRF3 deficiency in a patient with herpes simplex encephalitis. *J Exp Med* 212:1371-1379.

Bakkali, N., F. Fenollar, S. Biswas, J.M. Rolain, and D. Raoult. 2008. Acquired resistance to trimethoprim-sulfamethoxazole during Whipple disease and expression of the causative target gene. *J Infect Dis* 198:101-108.

Barreiro, L.B., and L. Quintana-Murci. 2010. From evolutionary genetics to human immunology: how selection shapes host defence genes. *Nature reviews. Genetics* 11:17-30.

Belkadi, A., V. Pedergnana, A. Cobat, Y. Itan, Q.B. Vincent, A. Abhyankar, L. Shang, J. El Baghdadi, A. Bousfiha, A. Alcais, B. Boisson, J.L. Casanova, and L. Abel. 2016. Whole-exome sequencing to analyze population structure, parental inbreeding, and familial linkage. *Proc Natl Acad Sci U S A* 113:6713-6718.

Bogunovic, D., M. Byun, L.A. Durfee, A. Abhyankar, O. Sanal, D. Mansouri, S. Salem, I. Radovanovic, A.V. Grant, P. Adimi, N. Mansouri, S. Okada, V.L. Bryant, X.F. Kong, A. Kreins, M.M. Velez, B. Boisson, S. Khalilzadeh, U. Ozcelik, I.A. Darazam, J.W. Schoggins, C.M. Rice, S. Al-Muhsen, M. Behr, G. Vogt, A. Puel, J. Bustamante, P. Gros, J.M. Huibregtse, L. Abel, S. Boisson-Dupuis, and J.L. Casanova. 2012. Mycobacterial Disease and Impaired IFN-gamma Immunity in Humans with Inherited ISG15 Deficiency. *Science*

Brass, A.L., A.Q. Zhu, and H. Singh. 1999. Assembly requirements of PU.1-Pip (IRF-4) activator complexes: inhibiting function in vivo using fused dimers. *EMBO J* 18:977-991.

Braubach, P., T. Lippmann, D. Raoult, J.C. Lagier, I. Anagnostopoulos, S. Zender, F.P. Langer, H.H. Kreipe, M.P. Kuhnel, and D. Jonigk. 2017. Fluorescence In Situ Hybridization for Diagnosis of Whipple's Disease in Formalin-Fixed Paraffin-Embedded Tissue. *Frontiers in medicine* 4:87.

Bujko, A., N. Atlasy, O.J.B. Landsverk, L. Richter, S. Yaqub, R. Horneland, O. Oyen, E.M. Aandahl, L. Aabakken, H.G. Stunnenberg, E.S. Baekkevold, and F.L. Jahnsen. 2017. Transcriptional and functional profiling defines human small intestinal macrophage subsets. *J Exp Med*

Byun, M., A. Abhyankar, V. Lelarge, S. Plancoulaine, A. Palanduz, L. Telhan, B. Boisson, C. Picard, S. Dewell, C. Zhao, E. Jouanguy, S. Feske, L. Abel, and J.L. Casanova. 2010. Whole-exome sequencing-based discovery of STIM1 deficiency in a child with fatal classic Kaposi sarcoma. *J Exp Med* 207:2307-2312.

770 Casanova, J.L. 2015a. Human genetic basis of interindividual variability in the course of infection. *Proc*
771 *Natl Acad Sci U S A* 112:E7118-7127.
772 Casanova, J.L. 2015b. Severe infectious diseases of childhood as monogenic inborn errors of
773 immunity. *Proc Natl Acad Sci U S A* 112:E7128-7137.
774 Ciancanelli, M.J., S.X. Huang, P. Luthra, H. Garner, Y. Itan, S. Volpi, F.G. Lafaille, C. Trouillet, M.
775 Schmolke, R.A. Albrecht, E. Israelsson, H.K. Lim, M. Casadio, T. Hermesh, L. Lorenzo, L.W.
776 Leung, V. Pedergnana, B. Boisson, S. Okada, C. Picard, B. Ringuier, F. Troussier, D. Chaussabel,
777 L. Abel, I. Pellier, L.D. Notarangelo, A. Garcia-Sastre, C.F. Basler, F. Geissmann, S.Y. Zhang,
778 H.W. Snoeck, and J.L. Casanova. 2015. Infectious disease. Life-threatening influenza and
779 impaired interferon amplification in human IRF7 deficiency. *Science* 348:448-453.
780 Desnues, B., K. Al Moussawi, and F. Fenollar. 2010. New insights into Whipple's disease and
781 Tropheryma whipplei infections. *Microbes Infect* 12:1102-1110.
782 Dobbins, W.O., 3rd. 1981. Is there an immune deficit in Whipple's disease? *Digestive diseases and*
783 *sciences* 26:247-252.
784 Dobbins, W.O.I. 1987. Whipple's disease. *Thomas Books* Springfield, IL:
785 Durand, D.V., C. Lecomte, P. Cathebras, H. Rousset, and P. Godeau. 1997. Whipple disease. Clinical
786 review of 52 cases. The SNFMI Research Group on Whipple Disease. Societe Nationale
787 Francaise de Medecine Interne. *Medicine (Baltimore)* 76:170-184.
788 Edouard, S., F. Fenollar, and D. Raoult. 2012. The rise of Tropheryma whipplei: a 12-year
789 retrospective study of PCR diagnoses in our reference center. *J Clin Microbiol* 50:3917-3920.
790 Ehrbar, H.U., P. Bauerfeind, F. Dutly, H.R. Koelz, and M. Altwegg. 1999. PCR-positive tests for
791 Tropheryma whippelii in patients without Whipple's disease. *Lancet* 353:2214.
792 Eilertson, K.E., J.G. Booth, and C.D. Bustamante. 2012. SnIPRE: selection inference using a Poisson
793 random effects model. *PLoS computational biology* 8:e1002806.
794 Escalante, C.R., A.L. Brass, J.M. Pongubala, E. Shatova, L. Shen, H. Singh, and A.K. Aggarwal. 2002.
795 Crystal structure of PU.1/IRF-4/DNA ternary complex. *Mol Cell* 10:1097-1105.
796 Fenollar, F., B. Amphoux, and D. Raoult. 2009. A paradoxical Tropheryma whipplei western blot
797 differentiates patients with whipple disease from asymptomatic carriers. *Clin Infect Dis*
798 49:717-723.
799 Fenollar, F., J.C. Lagier, and D. Raoult. 2014. Tropheryma whipplei and Whipple's disease. *J Infect*
800 69:103-112.
801 Fenollar, F., S. Laouira, H. Lepidi, J.M. Rolain, and D. Raoult. 2008a. Value of Tropheryma whipplei
802 quantitative polymerase chain reaction assay for the diagnosis of Whipple disease:
803 usefulness of saliva and stool specimens for first-line screening. *Clin Infect Dis* 47:659-667.
804 Fenollar, F., H. Lepidi, and D. Raoult. 2001. Whipple's endocarditis: review of the literature and
805 comparisons with Q fever, Bartonella infection, and blood culture-positive endocarditis. *Clin*
806 *Infect Dis* 33:1309-1316.
807 Fenollar, F., X. Puechal, and D. Raoult. 2007. Whipple's disease. *N Engl J Med* 356:55-66.
808 Fenollar, F., M. Trani, B. Davoust, B. Salle, M.L. Birg, J.M. Rolain, and D. Raoult. 2008b. Prevalence of
809 asymptomatic Tropheryma whipplei carriage among humans and nonhuman primates. *J*
810 *Infect Dis* 197:880-887.
811 Fleming, J.L., R.H. Wiesner, and R.G. Shorter. 1988. Whipple's disease: clinical, biochemical, and
812 histopathologic features and assessment of treatment in 29 patients. *Mayo Clinic*
813 *proceedings* 63:539-551.
814 Gautier, L., L. Cope, B.M. Bolstad, and R.A. Irizarry. 2004. affy--analysis of Affymetrix GeneChip data
815 at the probe level. *Bioinformatics* 20:307-315.
816 Gubler, J.G., M. Kuster, F. Dutly, F. Bannwart, M. Krause, H.P. Vogelin, G. Garzoli, and M. Altwegg.
817 1999. Whipple endocarditis without overt gastrointestinal disease: report of four cases. *Ann*
818 *Intern Med* 131:112-116.
819 Ikushima, H., H. Negishi, and T. Taniguchi. 2013. The IRF family transcription factors at the interface
820 of innate and adaptive immune responses. *Cold Spring Harbor symposia on quantitative*
821 *biology* 78:105-116.

Irizarry, R.A., B. Hobbs, F. Collin, Y.D. Beazer-Barclay, K.J. Antonellis, U. Scherf, and T.P. Speed. 2003. Exploration, normalization, and summaries of high density oligonucleotide array probe level data. *Biostatistics* 4:249-264.

Israel, L., Y. Wang, K. Bulek, E. Della Mina, Z. Zhang, V. Pedergnana, M. Chrabieh, N.A. Lemmens, V. Sancho-Shimizu, M. Descatoire, T. Lasseau, E. Israelsson, L. Lorenzo, L. Yun, A. Belkadi, A. Moran, L.E. Weisman, F. Vandenesch, F. Batteux, S. Weller, M. Levin, J. Herberg, A. Abhyankar, C. Prando, Y. Itan, W.J.B. van Wamel, C. Picard, L. Abel, D. Chaussabel, X. Li, B. Beutler, P.D. Arkwright, J.L. Casanova, and A. Puel. 2017. Human Adaptive Immunity Rescues an Inborn Error of Innate Immunity. *Cell* 168:789-800 e710.

Itan, Y., L. Shang, B. Boisson, M.J. Ciancanelli, J.G. Markle, R. Martinez-Barricarte, E. Scott, I. Shah, P.D. Stenson, J. Gleeson, D.N. Cooper, L. Quintana-Murci, S.Y. Zhang, L. Abel, and J.L. Casanova. 2016. The mutation significance cutoff: gene-level thresholds for variant predictions. *Nature methods* 13:109-110.

Itan, Y., L. Shang, B. Boisson, E. Patin, A. Bolze, M. Moncada-Velez, E. Scott, M.J. Ciancanelli, F.G. Lafaille, J.G. Markle, R. Martinez-Barricarte, S.J. de Jong, X.F. Kong, P. Nitschke, A. Belkadi, J. Bustamante, A. Puel, S. Boisson-Dupuis, P.D. Stenson, J.G. Gleeson, D.N. Cooper, L. Quintana-Murci, J.M. Claverie, S.Y. Zhang, L. Abel, and J.L. Casanova. 2015. The human gene damage index as a gene-level approach to prioritizing exome variants. *Proc Natl Acad Sci U S A* 112:13615-13620.

Kircher, M., D.M. Witten, P. Jain, B.J. O'Roak, G.M. Cooper, and J. Shendure. 2014. A general framework for estimating the relative pathogenicity of human genetic variants. *Nat Genet* 46:310-315.

Klein, U., S. Casola, G. Cattoretti, Q. Shen, M. Lia, T. Mo, T. Ludwig, K. Rajewsky, and R. Dalla-Favera. 2006. Transcription factor IRF4 controls plasma cell differentiation and class-switch recombination. *Nat Immunol* 7:773-782.

Lagier, J.C., F. Fenollar, H. Lepidi, and D. Raoult. 2010. Failure and relapse after treatment with trimethoprim/sulfamethoxazole in classic Whipple's disease. *J Antimicrob Chemother* 65:2005-2012.

Lagier, J.C., F. Fenollar, H. Lepidi, and D. Raoult. 2011. Evidence of lifetime susceptibility to Tropheryma whipplei in patients with Whipple's disease. *J Antimicrob Chemother* 66:1188-1189.

Lamborn, I.T., H. Jing, Y. Zhang, S.B. Drutman, J.K. Abbott, S. Munir, S. Bade, H.M. Murdock, C.P. Santos, L.G. Brock, E. Masutani, E.Y. Fordjour, J.J. McElwee, J.D. Hughes, D.P. Nichols, A. Belkadi, A.J. Oler, C.S. Happel, H.F. Matthews, L. Abel, P.L. Collins, K. Subbarao, E.W. Gelfand, M.J. Ciancanelli, J.L. Casanova, and H.C. Su. 2017. Recurrent rhinovirus infections in a child with inherited MDA5 deficiency. *J Exp Med* 214:1949-1972.

Lau, J.F., J.P. Parisien, and C.M. Horvath. 2000. Interferon regulatory factor subcellular localization is determined by a bipartite nuclear localization signal in the DNA-binding domain and interaction with cytoplasmic retention factors. *Proc Natl Acad Sci U S A* 97:7278-7283.

Lek, M., K.J. Karczewski, E.V. Minikel, K.E. Samocha, E. Banks, T. Fennell, A.H. O'Donnell-Luria, J.S. Ware, A.J. Hill, B.B. Cummings, T. Tukiainen, D.P. Birnbaum, J.A. Kosmicki, L.E. Duncan, K. Estrada, F. Zhao, J. Zou, E. Pierce-Hoffman, J. Berghout, D.N. Cooper, N. Deflaux, M. DePristo, R. Do, J. Flannick, M. Fromer, L. Gauthier, J. Goldstein, N. Gupta, D. Howrigan, A. Kiezun, M.I. Kurki, A.L. Moonshine, P. Natarajan, L. Orozco, G.M. Peloso, R. Poplin, M.A. Rivas, V. Ruano-Rubio, S.A. Rose, D.M. Ruderfer, K. Shakir, P.D. Stenson, C. Stevens, B.P. Thomas, G. Tiao, M.T. Tusie-Luna, B. Weisburd, H.H. Won, D. Yu, D.M. Altshuler, D. Ardissino, M. Boehnke, J. Danesh, S. Donnelly, R. Elosua, J.C. Florez, S.B. Gabriel, G. Getz, S.J. Glatt, C.M. Hultman, S. Kathiresan, M. Laakso, S. McCarroll, M.I. McCarthy, D. McGovern, R. McPherson, B.M. Neale, A. Palotie, S.M. Purcell, D. Saleheen, J.M. Scharf, P. Sklar, P.F. Sullivan, J. Tuomilehto, M.T. Tsuang, H.C. Watkins, J.G. Wilson, M.J. Daly, and D.G. MacArthur. 2016. Analysis of protein-coding genetic variation in 60,706 humans. *Nature* 536:285-291.

Lenardo, M., B. Lo, and C.L. Lucas. 2016. Genomics of Immune Diseases and New Therapies. *Annu Rev Immunol* 34:121-149.
Li, H., and R. Durbin. 2009. Fast and accurate short read alignment with Burrows-Wheeler transform. *Bioinformatics* 25:1754-1760.
Li, H., B. Handsaker, A. Wysoker, T. Fennell, J. Ruan, N. Homer, G. Marth, G. Abecasis, and R. Durbin. 2009. The Sequence Alignment/Map format and SAMtools. *Bioinformatics* 25:2078-2079.
Li, P., R. Spolski, W. Liao, L. Wang, T.L. Murphy, K.M. Murphy, and W.J. Leonard. 2012. BATF-JUN is critical for IRF4-mediated transcription in T cells. *Nature* 490:543-546.
Li, W., F. Fenollar, J.M. Rolain, P.E. Fournier, G.E. Feurle, C. Muller, V. Moos, T. Marth, M. Altwegg, R.C. Calligaris-Maibach, T. Schneider, F. Biagi, B. La Scola, and D. Raoult. 2008. Genotyping reveals a wide heterogeneity of Tropheryma whipplei. *Microbiology* 154:521-527.
Lohoff, M., H.W. Mittrucker, S. Prechtl, S. Bischof, F. Sommer, S. Kock, D.A. Ferrick, G.S. Duncan, A. Gessner, and T.W. Mak. 2002. Dysregulated T helper cell differentiation in the absence of interferon regulatory factor 4. *Proc Natl Acad Sci U S A* 99:11808-11812.
Ma, C.S., D.T. Avery, A. Chan, M. Batten, J. Bustamante, S. Boisson-Dupuis, P.D. Arkwright, A.Y. Kreins, D. Averbuch, D. Engelhard, K. Magdorf, S.S. Kilic, Y. Minegishi, S. Nonoyama, M.A. French, S. Choo, J.M. Smart, J. Peake, M. Wong, P. Gray, M.C. Cook, D.A. Fulcher, J.L. Casanova, E.K. Deenick, and S.G. Tangye. 2012. Functional STAT3 deficiency compromises the generation of human T follicular helper cells. *Blood* 119:3997-4008.
Ma, C.S., N. Wong, G. Rao, A. Nguyen, D.T. Avery, K. Payne, J. Torpy, P. O'Young, E. Deenick, J. Bustamante, A. Puel, S. Okada, M. Kobayashi, R. Martinez-Barricarte, M. Elliott, S. Sebnem Kilic, J. El Baghdadi, Y. Minegishi, A. Bousfiha, N. Robertson, S. Hambleton, P.D. Arkwright, M. French, A.K. Blincoe, P. Hsu, D.E. Campbell, M.O. Stormon, M. Wong, S. Adelstein, D.A. Fulcher, M.C. Cook, P. Stepensky, K. Boztug, R. Beier, A. Ikinciogullari, J.B. Ziegler, P. Gray, C. Picard, S. Boisson-Dupuis, T.G. Phan, B. Grimbacher, K. Warnatz, S.M. Holland, G. Uzel, J.L. Casanova, and S.G. Tangye. 2016. Unique and shared signaling pathways cooperate to regulate the differentiation of human CD4+ T cells into distinct effector subsets. *J Exp Med* 213:1589-1608.
Mahnel, R., A. Kalt, S. Ring, A. Stallmach, W. Strober, and T. Marth. 2005. Immunosuppressive therapy in Whipple's disease patients is associated with the appearance of gastrointestinal manifestations. *Am J Gastroenterol* 100:1167-1173.
Maibach, R.C., F. Dutly, and M. Altwegg. 2002. Detection of Tropheryma whipplei DNA in feces by PCR using a target capture method. *J Clin Microbiol* 40:2466-2471.
Maizel, H., J.M. Ruffin, and W.O. Dobbins, 3rd. 1970. Whipple's disease: a review of 19 patients from one hospital and a review of the literature since 1950. *Medicine (Baltimore)* 49:175-205.
Marth, T., V. Moos, C. Muller, F. Biagi, and T. Schneider. 2016. Tropheryma whipplei infection and Whipple's disease. *Lancet Infect Dis* 16:e13-22.
Marumganti, A.R., and T.F. Murphy. 2008. Whipple's disease: neurological relapse presenting as headache for two years. *Journal of general internal medicine* 23:2131-2133.
McKenna, A., M. Hanna, E. Banks, A. Sivachenko, K. Cibulskis, A. Kernytsky, K. Garimella, D. Altshuler, S. Gabriel, M. Daly, and M.A. DePristo. 2010. The Genome Analysis Toolkit: a MapReduce framework for analyzing next-generation DNA sequencing data. *Genome Res* 20:1297-1303.
Mittrucker, H.W., T. Matsuyama, A. Grossman, T.M. Kundig, J. Potter, A. Shahinian, A. Wakeham, B. Patterson, P.S. Ohashi, and T.W. Mak. 1997. Requirement for the transcription factor LSIRF/IRF4 for mature B and T lymphocyte function. *Science* 275:540-543.
Ogunjimi, B., S.Y. Zhang, K.B. Sorensen, K.A. Skipper, M. Carter-Timofte, G. Kerner, S. Luecke, T. Prabakaran, Y. Cai, J. Meester, E. Bartholomeus, N.A. Bolar, G. Vandeweyer, C. Claes, Y. Sillis, L. Lorenzo, R.A. Fiorenza, S. Boucherit, C. Dielman, S. Heynderickx, G. Elias, A. Kurotova, A.V. Auwera, L. Verstraete, L. Lagae, H. Verhelst, A. Jansen, J. Ramet, A. Suls, E. Smits, B. Ceulemans, L. Van Laer, G. Plat Wilson, J. Kreth, C. Picard, H. Von Bernuth, J. Fluss, S. Chabrier, L. Abel, G. Mortier, S. Fribourg, J.G. Mikkelsen, J.L. Casanova, S.R. Paludan, and T.H.

Mogensen. 2017. Inborn errors in RNA polymerase III underlie severe varicella zoster virus infections. *J Clin Invest* 127:3543-3556.

Perez de Diego, R., V. Sancho-Shimizu, L. Lorenzo, A. Puel, S. Plancoulaine, C. Picard, M. Herman, A. Cardon, A. Durandy, J. Bustamante, S. Vallabhapurapu, J. Bravo, K. Warnatz, Y. Chaix, F. Cascarrigny, P. Lebon, F. Rozenberg, M. Karin, M. Tardieu, S. Al-Muhsen, E. Jouanguy, S.Y. Zhang, L. Abel, and J.L. Casanova. 2010. Human TRAF3 adaptor molecule deficiency leads to impaired Toll-like receptor 3 response and susceptibility to herpes simplex encephalitis. *Immunity* 33:400-411.

Picard, C., H. Bobby Gaspar, W. Al-Herz, A. Bousfiha, J.L. Casanova, T. Chatila, Y.J. Crow, C. Cunningham-Rundles, A. Etzioni, J.L. Franco, S.M. Holland, C. Klein, T. Morio, H.D. Ochs, E. Oksenhendler, J. Puck, M.L.K. Tang, S.G. Tangye, T.R. Torgerson, and K.E. Sullivan. 2018. International Union of Immunological Societies: 2017 Primary Immunodeficiency Diseases Committee Report on Inborn Errors of Immunity. *J Clin Immunol* 38:96-128.

Ponz de Leon, M., A. Borghi, F. Ferrara, M. Contri, and L. Roncucci. 2006. Whipple's disease in a father-son pair. *Internal and emergency medicine* 1:254-256.

Puechal, X. 2016. Whipple's arthritis. *Joint, bone, spine : revue du rhumatisme* 83:631-635.

Purcell, S., B. Neale, K. Todd-Brown, L. Thomas, M.A. Ferreira, D. Bender, J. Maller, P. Sklar, P.I. de Bakker, M.J. Daly, and P.C. Sham. 2007. PLINK: a tool set for whole-genome association and population-based linkage analyses. *Am J Hum Genet* 81:559-575.

Quintana-Murci, L., and A.G. Clark. 2013. Population genetic tools for dissecting innate immunity in humans. *Nat Rev Immunol* 13:280-293.

Raoult, D., M.L. Birg, B. La Scola, P.E. Fournier, M. Enea, H. Lepidi, V. Roux, J.C. Piette, F. Vandenesch, D. Vital-Durand, and T.J. Marrie. 2000. Cultivation of the bacillus of Whipple's disease. *N Engl J Med* 342:620-625.

Relman, D.A., T.M. Schmidt, R.P. MacDermott, and S. Falkow. 1992. Identification of the uncultured bacillus of Whipple's disease. *N Engl J Med* 327:293-301.

Rieux-Laucat, F., and J.L. Casanova. 2014. Immunology. Autoimmunity by haploinsufficiency. *Science* 345:1560-1561.

Rolain, J.M., F. Fenollar, and D. Raoult. 2007. False positive PCR detection of Tropheryma whipplei in the saliva of healthy people. *BMC Microbiol* 7:48.

Schneider, T., V. Moos, C. Loddenkemper, T. Marth, F. Fenollar, and D. Raoult. 2008. Whipple's disease: new aspects of pathogenesis and treatment. *Lancet Infect Dis* 8:179-190.

Shaffer, A.L., N.C. Emre, P.B. Romesser, and L.M. Staudt. 2009. IRF4: Immunity. Malignancy! Therapy? *Clinical cancer research : an official journal of the American Association for Cancer Research* 15:2954-2961.

Street, S., H.D. Donoghue, and G.H. Neild. 1999. Tropheryma whippelii DNA in saliva of healthy people. *Lancet* 354:1178-1179.

Suzuki, S., K. Honma, T. Matsuyama, K. Suzuki, K. Toriyama, I. Akitoyo, K. Yamamoto, T. Suematsu, M. Nakamura, K. Yui, and A. Kumatori. 2004. Critical roles of interferon regulatory factor 4 in CD11bhighCD8alpha- dendritic cell development. *Proc Natl Acad Sci U S A* 101:8981-8986.

Tamura, T., P. Tailor, K. Yamaoka, H.J. Kong, H. Tsujimura, J.J. O'Shea, H. Singh, and K. Ozato. 2005. IFN regulatory factor-4 and -8 govern dendritic cell subset development and their functional diversity. *J Immunol* 174:2573-2581.

Tominaga, N., K. Ohkusu-Tsukada, H. Udono, R. Abe, T. Matsuyama, and K. Yui. 2003. Development of Th1 and not Th2 immune responses in mice lacking IFN-regulatory factor-4. *International immunology* 15:1-10.

Vanhollebeke, B., P. Truc, P. Poelvoorde, A. Pays, P.P. Joshi, R. Katti, J.G. Jannin, and E. Pays. 2006. Human Trypanosoma evansi infection linked to a lack of apolipoprotein L-I. *N Engl J Med* 355:2752-2756.

Wang, K., M. Li, and H. Hakonarson. 2010. ANNOVAR: functional annotation of genetic variants from high-throughput sequencing data. *Nucleic acids research* 38:e164.

Whipple, G.H. 1907. A hitherto undescribed disease characterized anatomically by deposits of fat and fattyacids in the intestinal and mesentericlymphatic tissues. *Bull. Johns Hopkins Hosp.* 18:382.

Yardley, J.H., and T.R. Hendrix. 1961. Combined electron and light microscopy in Whipple's disease. Demonstration of "bacillary bodies" in the intestine. *Bull Johns Hopkins Hosp* 109:80-98.

Zhang, S.Y., N.E. Clark, C.A. Freije, E. Pauwels, A.J. Taggart, S. Okada, H. Mandel, P. Garcia, M.J. Ciancanelli, A. Biran, F.G. Lafaille, M. Tsumura, A. Cobat, J. Luo, S. Volpi, B. Zimmer, S. Sakata, A. Dinis, O. Ohara, E.J. Garcia Reino, K. Dobbs, M. Hasek, S.P. Holloway, K. McCammon, S.A. Hussong, N. DeRosa, C.E. Van Skike, A. Katolik, L. Lorenzo, M. Hyodo, E. Faria, R. Halwani, R. Fukuhara, G.A. Smith, V. Galvan, M.J. Damha, S. Al-Muhsen, Y. Itan, J.D. Boeke, L.D. Notarangelo, L. Studer, M. Kobayashi, L. Diogo, W.G. Fairbrother, L. Abel, B.R. Rosenberg, P.J. Hart, A. Etzioni, and J.L. Casanova. 2018. Inborn Errors of RNA Lariat Metabolism in Humans with Brainstem Viral Infection. *Cell* 172:952-965 e918.

Figure legends

Figure 1. Autosomal dominant IRF4 deficiency. **A.** Pedigree of the kindred, with allele segregation. Generations are designated by Roman numerals (I, II, III, IV, V and VI), and each individual is designated by an Arabic numeral (from left to right). Each symbol is divided into two parts: the upper part indicates clinical status for WD (black: affected, white: healthy, "?": not known), the lower part indicates whether Tw was identified by PCR (in saliva, blood, feces or joint fluid) or by PAS staining on bowel biopsy specimens (gray: Tw-positive, white: Tw-negative, "?": not tested). Whipple's disease patients are indicated as P1, P2, P3, and P4; the proband is indicated with an arrow. Genotype status and age (for *IRF4*-heterozygous individuals) are reported below the symbols. Individuals whose genetic status could not be evaluated are indicated by the symbol "E?". **B.** Schematic representation of the IRF4 protein, showing the DNA-binding domain (DBD), P-rich domain, activation domain, α-helical domain, Q-rich domain, IFR association domain (IAD) and auto-inhibitory domain. The R98W substitution is indicated in red. **C.** Electropherogram of *IRF4* genomic DNA sequences from a healthy unrelated control (C) and the patients (P1, P2, P3, P4). The R98W *IRF4* mutation leads to the replacement of an arginine with a tryptophan residue in position 98 (exon 3, c.292 C>T). The corresponding amino acids are represented above each electropherogram. **D.** Alignment of the R98W amino acid in the DBD domain of IRF4 in humans and 11 other animal species. R98 is indicated in red.

Figure 1-figure supplement 1. Genome-wide linkage and whole-exome sequencing analyses. A. Genome-wide linkage analysis was performed by combining genome-wide array and whole-exome sequencing (WES) data, assuming an autosomal dominant (AD) mode of inheritance. LOD (logarithm of odds) scores are shown for the four patients considered

1015 together. The maximum expected LOD score is 1.95, based on an AD model with incomplete
1016 penetrance. *IRF4* is located within a linkage region (LOD=1.94) on chromosome 6 (indicated
1017 by a black arrow). **B.** A refined analysis of WES data identified *IRF4* as the only protein-
1018 coding gene carrying a rare heterozygous mutation common to P1, P2, P3 and P4 within the
1019 linkage regions.
1020
1021 **Figure 1-source data 1. Kindred information summary.** For each subject, Tw carriage
1022 status, *IRF4* genotype, clinical status and date of birth (DOB) are reported. NA: not available;
1023 Pos: positive; Neg: negative; Tw: *Tropheryma whipplei*; WD: Whipple's disease; E?:
1024 genotype not assessed.
1025
1026 **Figure 1-source data 2. Non-synonymous variants within the linkage regions found in**
1027 **WES data from patients.**
1028
1029 **Figure 2**. **Analysis *in silico* of *IRF4* variants**. **A.** Minor allele frequency and combined
1030 annotation–dependent depletion score (CADD) of all coding variants previously reported in a
1031 public database (gnomAD) (http://gnomad.broadinstitute.org) and in our in-house (HGID)
1032 database. The dotted line corresponds to the mutation significance cutoff (MSC) with 95%
1033 confidence interval. The R98W variant is shown as a red square.
1034
1035 **Figure 2-figure supplement 1. List of variants and strength of purifying selection on**
1036 ***IRF4*.** Genome-wide distribution of the strength of purifying selection, estimated by the *f*
1037 parameter (Eilertson et al., 2012), acting on 14,993 human genes. *IRF4* is at the 9.4th
1038 percentile of the distribution, indicating that it is more constrained than most human genes.
1039

Figure 2-source data 1. 156 non-synonymous heterozygous coding or splice variants reported in the gnomAD or HGID databases. †: non-canonical transcript predicted to undergo nonsense mediated decay.

Figure 3. Molecular characterization of the R98W *IRF4* mutation (loss of DNA binding). **A.** HEK293T cells were transfected with the pcDNA3.1 empty vector (E) or plasmids encoding *IRF4* WT, *IRF4* R98W or *IRF4* R98A-C99A. Total cell extracts were subjected to western blotting; the upper panel shows IRF4 levels and the lower panel shows the levels of GAPDH, used as a loading control. The results shown are representative of three independent experiments. **B.** (upper panel) HEK293T cells were transfected with the pcDNA3.1 empty vector (E) or plasmids encoding *IRF4* WT or *IRF4* R98W . Total cell (1), cytoplasmic (2) and nuclear (3) extracts were subjected to western blotting. Lamin A/C and GAPDH were used as loading controls. (lower panel) IRF4 signal intensity for R98W-transfected cells and WT-transfected cells, in various cell compartments (total, cytoplasmic and nuclear), normalized against the GAPDH signal, as shown by western blotting. The results shown are representative of three independent experiments. **C**. Luciferase activity of HEK293T cells cotransfected with an $(ISRE)_3$ reporter plasmid plus the pcDNA3.1 empty vector (E, 100 ng) and various amounts of plasmids encoding *IRF4* WT or *IRF4* R98W or *IRF4* R98A/C99A (6.25 ng, 12.5 ng, 25 ng, 50 ng, 75 ng and 100 ng). Results are shown as the fold induction of activity relative to E-transfected cells. The red dotted line indicates mean activity for E-transfected cells. The mean and standard error of three experiments are shown. **D.** Luciferase activity of HEK293T cells cotransfected with an *AICE* reporter plasmid plus the pcDNA3.1 empty vector (E, 100 ng) and/or constant amounts of plasmids encoding *BATF* WT and *JUN* WT (25 ng each, AP-1) and/or various amounts of plasmids encoding *IRF4* WT or *IRF4* R98W or *IRF4* R98A/C99A (6.25 ng, 12.5 ng, 18.8 ng, 25 ng, 37.5 ng and 50 ng). Results are

shown as the fold induction of activity relative to E-transfected cells. The red dotted line indicates mean activity for AP-1-transfected cells. The mean and standard error of two experiments are shown. **E.** Electrophoretic mobility shift assay (EMSA) with nuclear extracts of HEK293T cells transfected with the pcDNA3.1 empty vector (E), or plasmids encoding *IRF4* WT or *IRF4* R98W. Extracts were incubated with a ^{32}P-labeled *ISRE* probe. Extracts were incubated with a specific anti-IRF4 antibody (S) to detect DNA-protein complex supershift, with an isotype control antibody (I) to demonstrate the specificity of the complex, and with no antibody (-), as a control. The results shown are representative of three independent experiments. **F.** EMSA of nuclear extracts of HEK293T cells transfected with the pcDNA3.1 empty vector (E), or plasmids encoding *PU.1*, *IRF4* WT, or *IRF4* R98W, or cotransfected with *PU.1* and *IRF4* WT or *PU.1* and *IRF4* R98W plasmids. Extracts were incubated with a ^{32}P-labeled λB probe (EICE). Extracts were incubated with a specific anti-IRF4 antibody (S) to detect DNA-protein complex supershift, with an isotype control antibody (I) to demonstrate the IRF4 specificity of the complex and with no antibody (-), as a control. Experiments in the presence of excess non-radioactive probe (cold probe) demonstrated the probe specificity of the complexes. The results shown are representative of three independent experiments.

Figure 3-figure supplement 1. **Functional activity of IRF4. A.** Luciferase activity of HEK293T cells cotransfected with an $(ISRE)_3$ reporter plasmid plus the pcDNA3.1 empty vector (E) and plasmids encoding *IRF4* WT and/or *IRF4* R98W or *IRF4* R98A/C99A. The amount of plasmid used for transfection (ng) is indicated on the figure. Results are showed as fold induction of activity relative to E-transfected cells. The red dotted line represents the mean activity for E-transfected cells. The mean and standard error of three experiments are shown. **B.** Luciferase activity of HEK293T cells cotransfected with an *AICE* reporter plasmid

plus the pcDNA3.1 empty vector (E) and/or constant amounts of plasmids encoding *BATF* WT and *JUN* WT (25 ng each, AP-1) and/or plasmids encoding *IRF4* WT and/or *IRF4* R98W or *IRF4* R98A/C99A. The amounts of plasmid used for tranfection (ng) are indicated on the figure. Results are shown as the fold induction of activity relative to E-transfected cells. The red dotted line indicates mean activity for AP-1-transfected cells. The mean and standard error of two experiments are shown.

Figure 3-figure supplement 2. Protein levels of *IRF4* variants previously reported in gnomAD database. HEK293T cells were transfected with the pcDNA3.1 empty vector (E), or plasmids encoding *IRF4* WT, *IRF4* R98W or several *IRF4* variants previously reported in the gnomAD database (see Figure 3-source data 1). Total cell extracts were subjected to western blotting; the upper panel shows IRF4 levels and the lower panel shows the levels of GAPDH, used as a loading control. The results shown are representative of at least two independent experiments.

Figure 3-figure supplement 3. Protein levels of *IRF4* variants from HGID database. HEK293T cells were transfected with the pcDNA3.1 empty vector (E), or plasmids encoding *IRF4* WT, *IRF4* R98W or *IRF4* variants from the HGID database (see Figure 3-source data 1). Total cell extracts were subjected to western blotting; the upper panel shows IRF4 levels and the lower panel shows the levels of GAPDH, used as a loading control. The results shown are representative of at least two independent experiments.

Figure 3-figure supplement 4. Functional impact of *IRF4* variants previously reported in gnomAD database. Luciferase activity of HEK293T cells cotransfected with an $(ISRE)_3$ reporter plasmid plus the pcDNA3.1 empty vector (E) and plasmids encoding *IRF4* WT, *IRF4*

R98W or several IRF4 variants previously reported in the gnomAD databases (see Figure 3-source data 1). Results are shown as the fold induction of activity relative to E-transfected cells. The red dotted line represents the mean fold induction in E-transfected cells. The results shown are the mean ± SD of at least two independent experiments.

Figure 3-figure supplement 5. Functional impact of *IRF4* variants from HGID database. Luciferase activity of HEK293T cells cotransfected with an $(ISRE)_3$ reporter plasmid plus the pcDNA3.1 empty vector (E) and plasmids encoding *IRF4* WT, *IRF4* R98W or *IRF4* variants from the HGID database (see Figure 3-source data 1). Results are shown as the fold induction of activity relative to E-transfected cells. The red dotted line represents the mean fold induction in E-transfected cells. The results shown are the mean ± SD of at least two independent experiments.

Figure 4. *IRF4* mRNA levels in EBV-B cells. A. Total RNA extracted from healthy unrelated controls (*n*=7; *IRF4* WT/WT), patients diagnosed with Whipple's disease (*n*=25; WT/WT for all coding exons of *IRF4*) not related to this kindred, healthy homozygous WT relatives (*n*=4, *IRF4* WT/WT), patients with monoallelic *IRF4* mutations (*n*=2; *IRF4* WT/R98W) and asymptomatic heterozygous relatives with monoallelic *IRF4* mutations (*n*=2; *IRF4* WT/R98W) was subjected to RT-qPCR for total *IRF4*. Data are displayed as 2-ΔΔCt after normalization according to endogenous *GUSB* control gene expression (ΔCt) and the mean of controls (ΔΔCt). The results shown are the mean ± SD of three independent experiments. **B.** Calculated frequency (%) of each mRNA (WT and R98W allele) obtained by the TA-cloning of cDNA generated from EBV-B cells from healthy unrelated controls (*n*=2),

healthy homozygous WT relatives (*n*=1), patients with monoallelic *IRF4* mutations (*n*=2) and asymptomatic heterozygous relatives with monoallelic *IRF4* mutations (*n*=1).

Figure 4-figure supplement 1. IRF4 protein levels in EBV-B cells. A.-C. (Left) Total cell (A), cytoplasmic (B) and nuclear (C) extracts from five healthy unrelated controls (C1 to C5), three homozygous WT relatives (WT1, WT2, WT3), three patients (P1 to P3) and one asymptomatic heterozygous relative from the kindred (HET1). Protein extracts from HEK293T cells transfected with the pcDNA3.1 empty vector (E), or plasmids encoding *IRF4* WT or *IRF4* R98W were used as controls for the specific band corresponding to IRF4. (Right) Representation of IRF4 signal intensity for each individual relative to the mean signal for healthy unrelated controls (*n*=5) obtained on western blotting (Figure 4-figure supplement 1A-C left) and represented by black dotted lines, with normalization against the GAPDH signal (total, cytoplasmic extracts) or the lamin A/C signal (nuclear extracts). The results shown are representative of two independent experiments.

Figure 5. IRF4 protein levels in $CD4^+$ T cells.

A.-C. (Left) Total-cell (A), cytoplasmic (B) and nuclear (C) extracts from $CD4^+$ T cells from four healthy unrelated controls (C1 to C4) and two patients (P1 and P3) stimulated with activating anti-CD2/CD3/CD28 monoclonal antibody-coated beads (Stim) or left unstimulated (NS). Protein extracts from HEK293T cells transfected with the pcDNA3.1 empty vector (E) or plasmids encoding *IRF4* WT plasmids were used as controls for the specific band corresponding to IRF4. (Right) Representation of IRF4 signal intensity for each individual, obtained by western blotting, with normalization against the GAPDH signal (total, cytoplasmic extracts) or the topoisomerase I signal (nuclear extracts).

Figure 5-figure supplement 1. IRF4 protein levels in PBMC subpopulations.

Total cell extracts from PBMC subpopulations ($CD3^+$ T cells, $CD56^+$ NK cells, $CD19^+$ B cells, $CD19^+CD27^+$ memory B cells, $CD19^+CD27^-$ naive B cells, $CD14^+$ monocytes) from two healthy unrelated controls were subjected to western blotting. The upper panel shows IRF4 levels and the lower panel shows the levels of GAPDH, used as a loading control. The results shown are representative of two independent experiments. We showed that IRF4 was produced in large amounts in total B lymphocytes ($CD19^+$), but also in naïve and memory B lymphocytes ($CD19^+CD27^-$ and $CD19^+CD27^+$, respectively). IRF4 was less strongly expressed in $CD3^+$ T lymphocytes and was not detectable in $CD14^+$ monocytes or $CD56^+$ natural killer (NK) cells.

Figure 5-figure supplement 2. Percentage of dendritic cells and monocyte subtypes within total PBMCs. A. Percentage of $CD11c^+$, myeloid dendritic cells (mDC1 and mDC2) and plasmacytoid dendritic cells (pDCs) (left), and monocyte subtypes (right) among total PBMCs from healthy unrelated controls, a patient (P1) and a homozygous WT relative (WT1). We showed that the frequencies of these subsets in P1 were similar to those in healthy controls **B.** Gating strategy to define the dendritic cell and monocyte subtypes.

Figure 5-figure supplement 3. IRF4 levels in controls and patient monocyte-derived macrophages. A. IRF4 protein levels, as determined by western blotting on total cell extracts from M2-like (left panel) or M1-like (right panel) monocyte-derived macrophages (MDMs) from two healthy unrelated controls (C1 and C2) and P1, either left non-stimulated (NS) or stimulated with IL-4 (for M2-like MDMs) or IFN-γ (for M1-like MDMs). We showed that IRF4 was present in similar amounts in MDMs from P1 and healthy unrelated controls,

regardless of the differentiation or activation conditions used. **B.** IRF4 signal intensity for each individual relative to the mean signal for controls on western blots.

Figure 5-figure supplement 4. Surface marker levels in controls and patient monocyte-derived macrophages. A.-B. CD11b, CD86, CD206, CD209 and HLA-DR mean fluorescence intensity (MFI) for M2-MDM (C) and M1-MDM (D) from P1 and two healthy unrelated controls (C1 and C2), either left non-stimulated (NS) or stimulated with IL-4 (for M2-like MDMs) or IFN-γ (for M1-like MDMs). We showed that CD11b, CD86, CD206, CD209 and HLA-DR expression levels were similar in MDMs from P1 and healthy unrelated controls.

Figure 5-figure supplement 5. Percentage of memory B cells in PBMCs from controls and patients. PBMCs from healthy unrelated controls and patients (P1, P2 and P3) were stained with antibodies against CD20, CD10 and CD27, IgM, IgD, IgG or IgA. Percentages of memory B cells ($CD20^+$ $CD10^-$ $CD27^+$) were determined, and the proportion of memory B cells that had undergone class switching to express IgM/IgD, IgG or IgA was then calculated. No significant differences were observed between healthy unrelated controls and patients.

Figure 5-figure supplement 6. *In vitro* differentiation of $CD4^+$ T cells from patients and controls. Naïve and memory $CD4^+$ T cells from healthy unrelated controls and patients (P2 and P3) were purified by sorting and cultured with TAE beads. The secretion of IL-2, IL-4, IL-5, IL-9, IL-10, IL-13, IL-17A, IL-17F, IL-22, IFN-γ and TNF-α was measured five days later. No significant differences were observed between healthy unrelated controls and patients.

Figure 5-figure supplement 7. *Ex vivo* cytokine production by CD4$^+$ memory T cells from patients and controls.

C. Naïve CD4$^+$ T cells from healthy unrelated controls and patients (P2 and P3) were stimulated with TAE beads alone or under Th1, Th2, Th17 or Tfh polarizing conditions. The production of IL-10, IL-21, IL-17A, IL-17F and IFN-γ was measured five days later, in the corresponding polarizing conditions. No significant differences were observed between healthy unrelated controls and patients.

Figure 5-source data 1. Immunophenotyping of patients (P1, P2 and P3) and a WT homozygous relative. All subjects had normal numbers and percentages of T, B, and NK cells for age.

Figure 6. Overall transcriptional responsiveness of PBMCs following *in vitro* exposure to Tw and BCG and pathway activity analysis for genes responsive to BCG exposure. A. The overall responsiveness of individual subjects following stimulation with BCG and Tw, relative to non-stimulated conditions (along the horizontal axis) is shown as a heatmap. For each individual and each stimulus, overall responsiveness was assessed on the basis of normalized counts of differentially expressed transcripts, as described in the corresponding material and methods section. Subjects were grouped by unsupervised hierarchical clustering. **B.** Enriched canonical pathways were ranked according to differences in mean activation *z*-score between genotypes (WT/WT individuals vs. WT/R98W individuals). The activation *z*-scores for each individual and pathway are shown as heat maps. Pathways predicted to be activated are depicted in orange, pathways predicted to be inhibited are depicted in blue. A lack of prediction concerning activation is depicted in white. Individuals are presented in columns, pathways in rows. The pathways are ranked from most different between genotypes

(at the top of the list) to the least different (at the bottom). The differences in mean activation *z*-scores between WT/WT and WT/R98W individuals for each pathway are depicted as bars to the right of the heat maps (the direction of difference is not shown). The Ingenuity Pathway Analysis (IPA) tool was used to generate a list of the most significant canonical pathways and their respective activation *z*-scores.

Figure 6-data source 1. Differentially expressed (DE) genes found to be responsive to BCG in homozygous WT subjects using the criteria described in the material and methods section. Genes are grouped by up- or down- regulation and ranked in alphabetical order.

Figure 6-data source 2. Differentially expressed (DE) genes found to be responsive to Tw in homozygous WT subjects using the criteria described in the material and methods section. Genes are grouped by up- or down- regulation and ranked in alphabetical order.

Figure 1

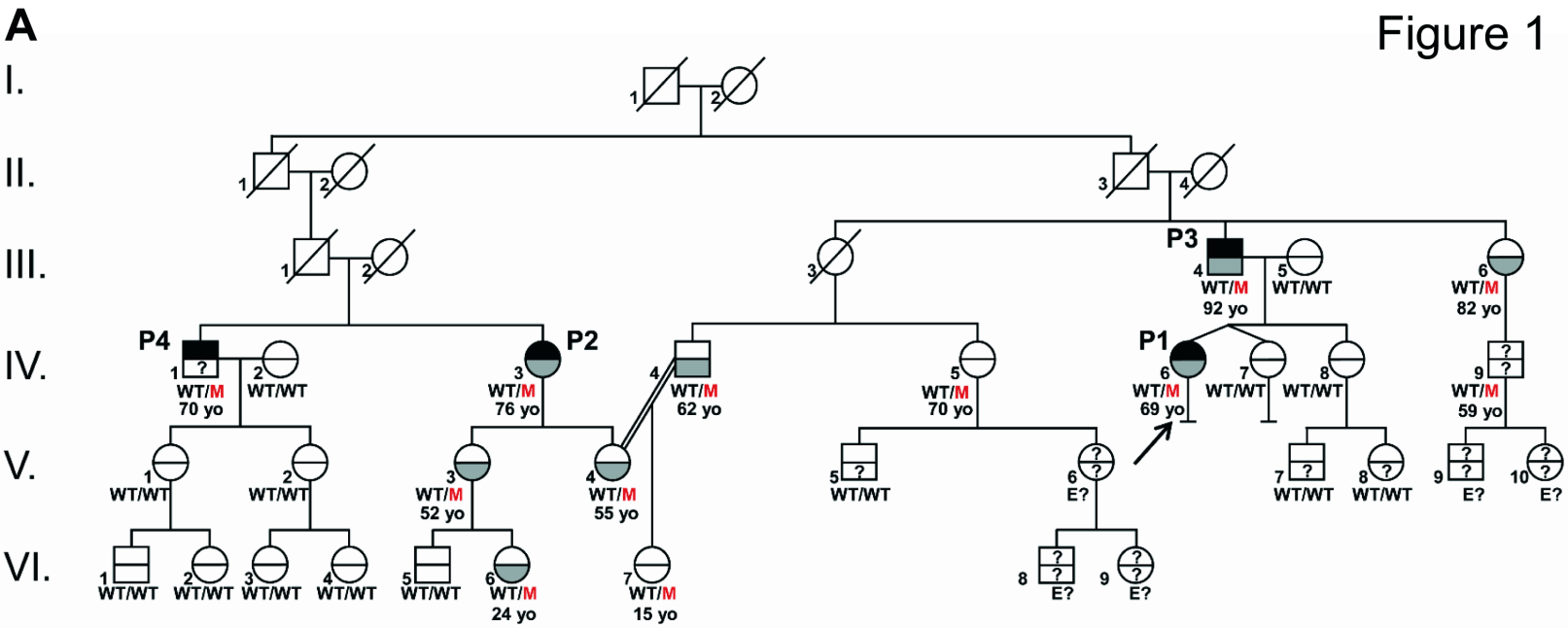

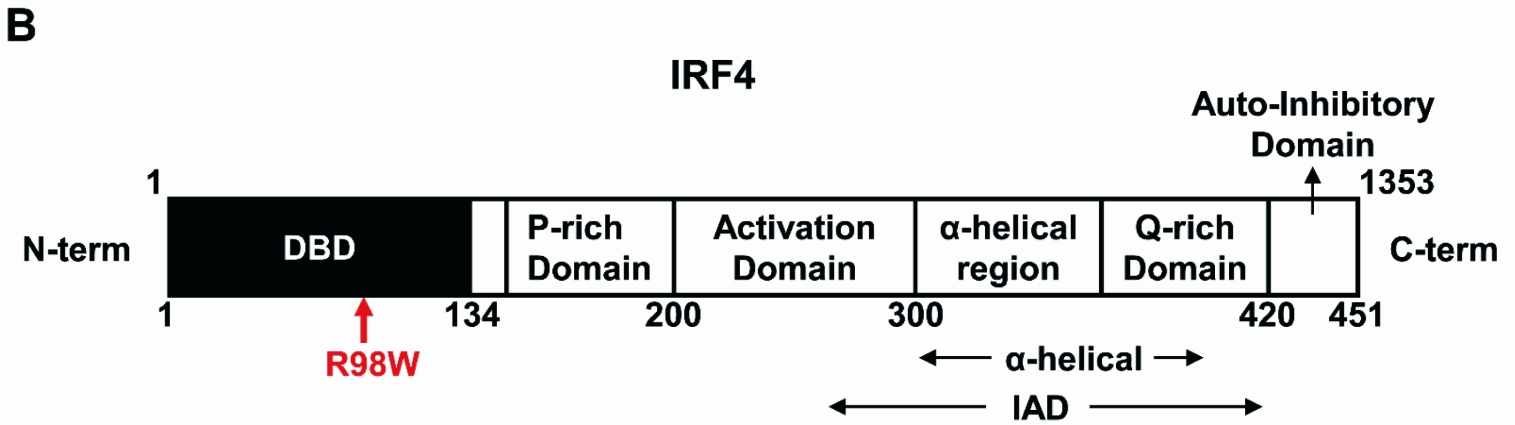

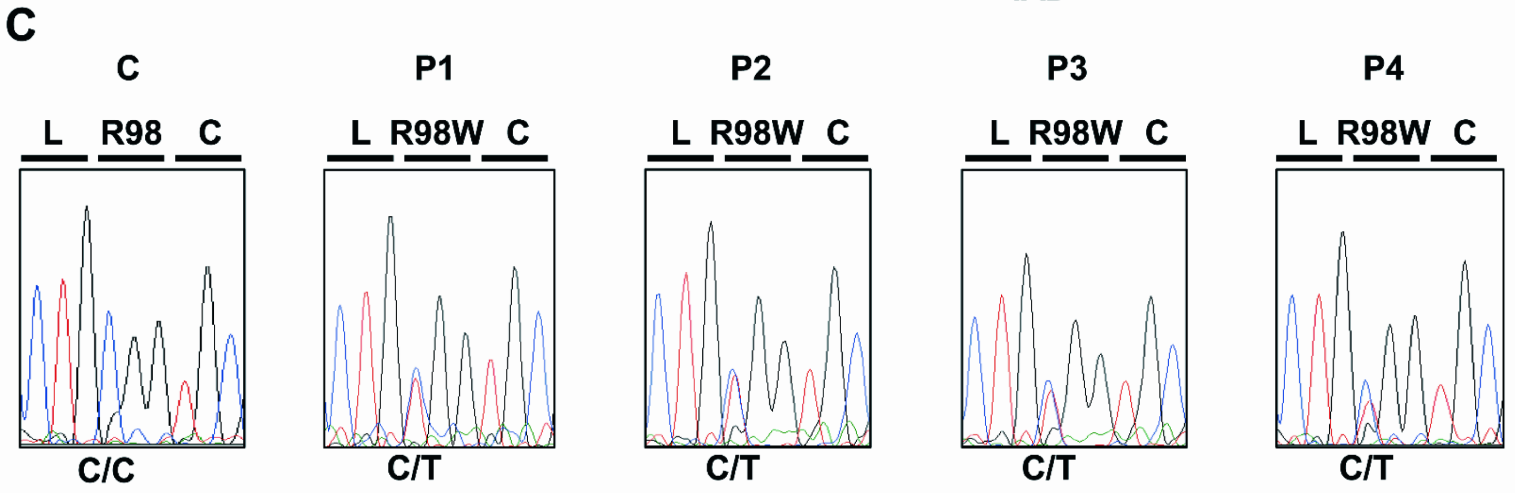

D

Homo sapiens	AWALFKGKFREGIDKPDPPTWKTRLRCALNKSNDFEELVERSQLDISDPYKVYRIVPEGAKKG
Pan troglodytes	AWALFKGKFREGIDKPDPPTWKTRLRCALNKSNDFEELVERSQLDISDPYKVYRIVPEGAKKG
Nomascus leucogenys	AWALFKGKFREGIDKPDPPTWKTRLRCALNKSNDFEELVERSQLDISDPYKVYRIVPEGAKKG
Macaca mulatta	AWALFKGKFREGIDKPDPPTWKTRLRCALNKSNDFEELVERSQLDISDPYKVYRIVPEGAKKG
Rattus norvegicus	AWALFKGKFREGIDKPDPPTWKTRLRCALNKSNDFEELVERSQLDISDPYKVYRIVPEGAKKG
Mus musculus	AWALFKGKFREGIDKPDPPTWKTRLRCALNKSNDFEELVERSQLDISDPYKVYRIVPEGAKKG
Canis familiaris	AWALFKGKFREGIDKPDPPTWKTRLRCALNKSNDFEELVERSQLDISDPYKVYRIVPEGAKKG
Ornithorhynchus anaticus	AWALFKGKFREGIDKPDPPTWKTRLRCALNKSNDFEELVERSQLDISDPYKVYRIVPEGAKKG
Gallus gallus	AWALFKGKFREGIDKPDPPTWKTRLRCALNKSNDFEELVERSQLDISDPYKVYRIVPEGAKKG
Xenopus tropicalis	AWALFKGKYREGIDKPDPPTWKTRLRCALNKSNDFEELVERSQLDISDPYKVYKIIPEGSKKG
Tetraodon nigroviridis	AWALFKGKFREGIDKPDPPTWKTRLRCALNKSNDFEELVDRSQLDISDPYKVYRIVPGGCQKK
Danio rerio	AWALFKGKFREGVDKPDPPTWKTRLRCALNKSNDFEEIVERSQLDISDPYKVYRIVPEGSKKG

Figure 1-figure supplement 1

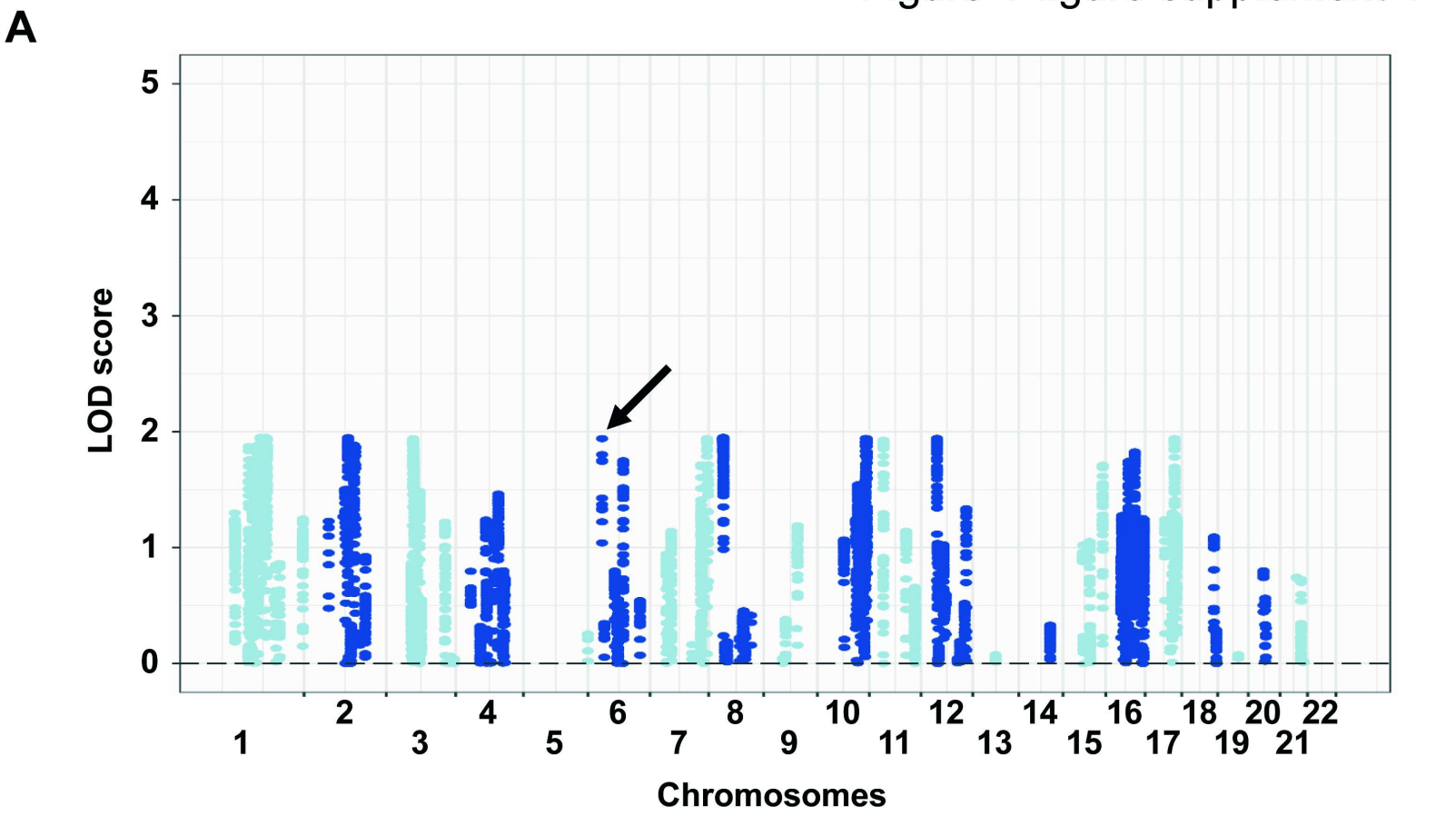

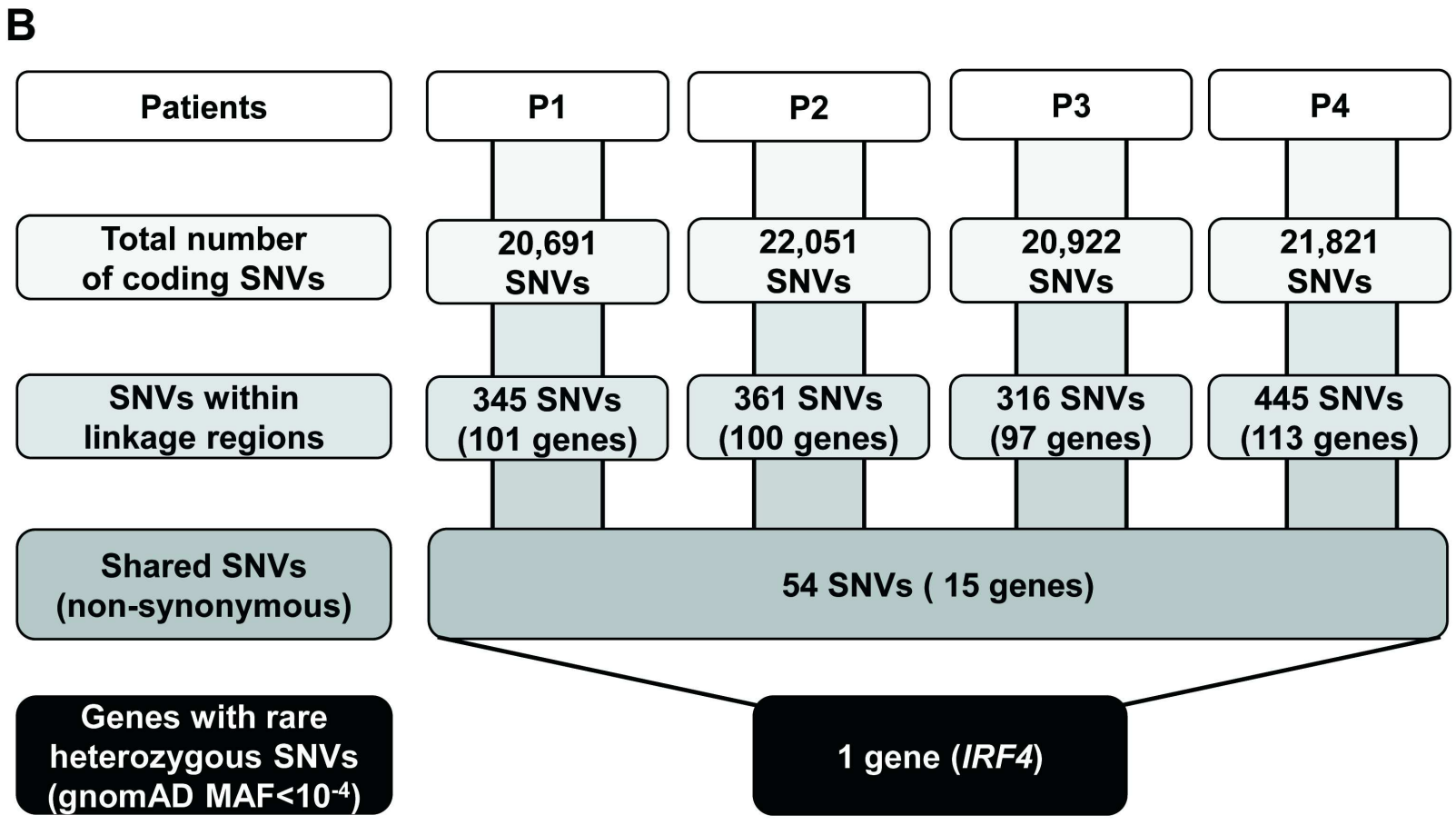

Figure 2

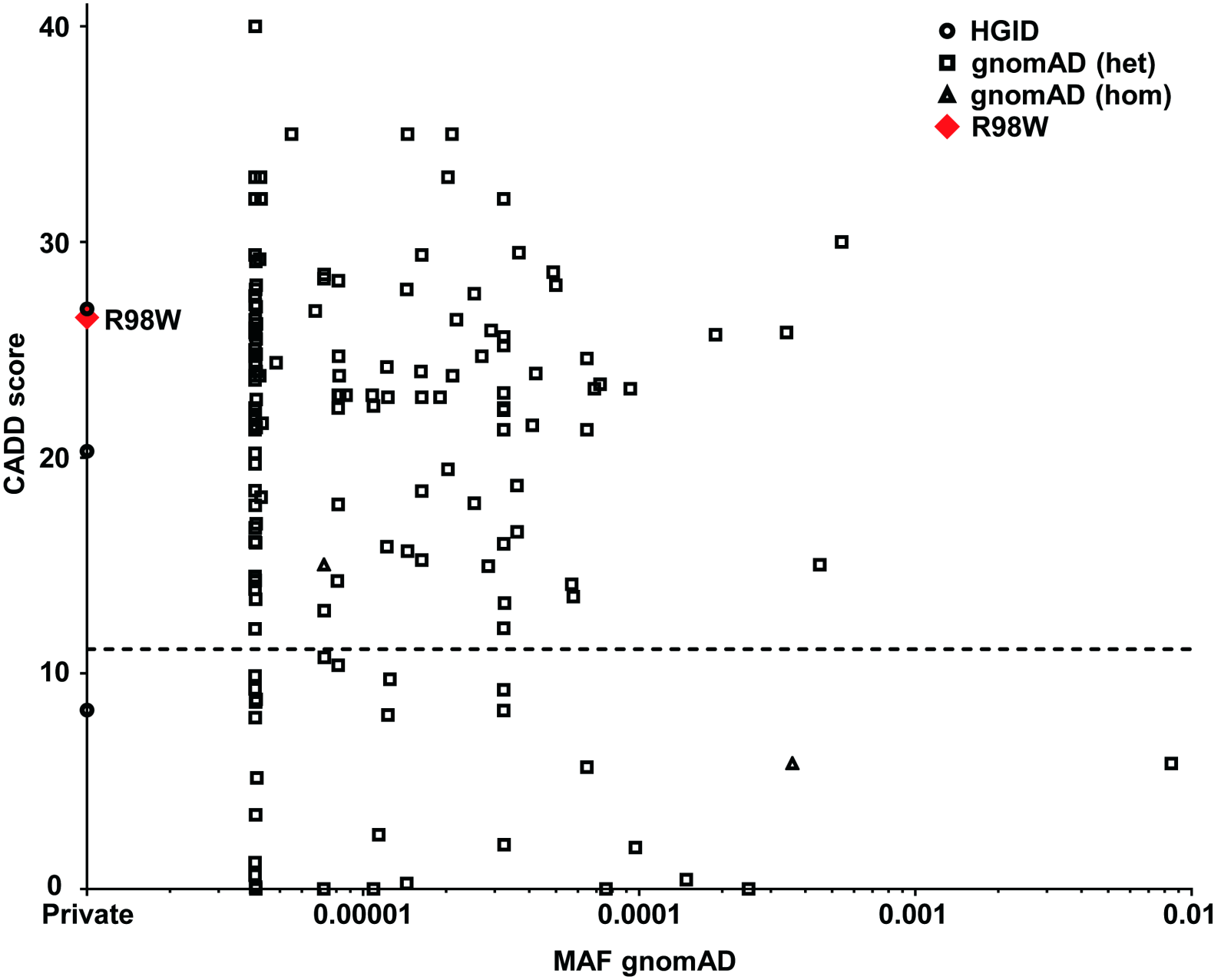
HGID
gnomAD (het)
gnomAD (hom)
R98W
CADD score
40
30
20
10
0
R98W
Private
0.00001
0.0001
0.001
0.01
MAF gnomAD

Figure 2-figure supplement 1

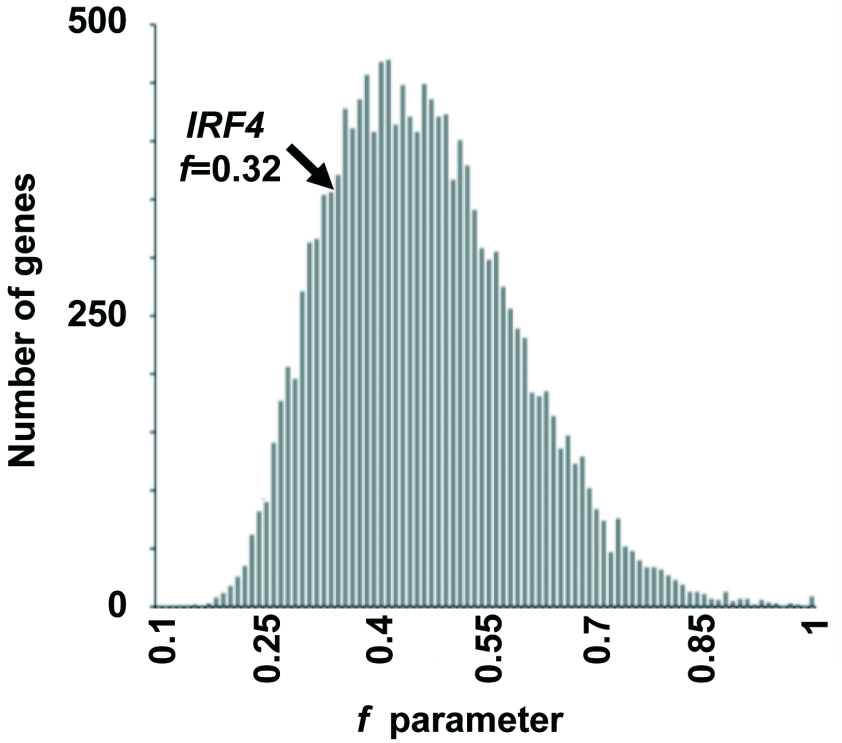

Figure 3

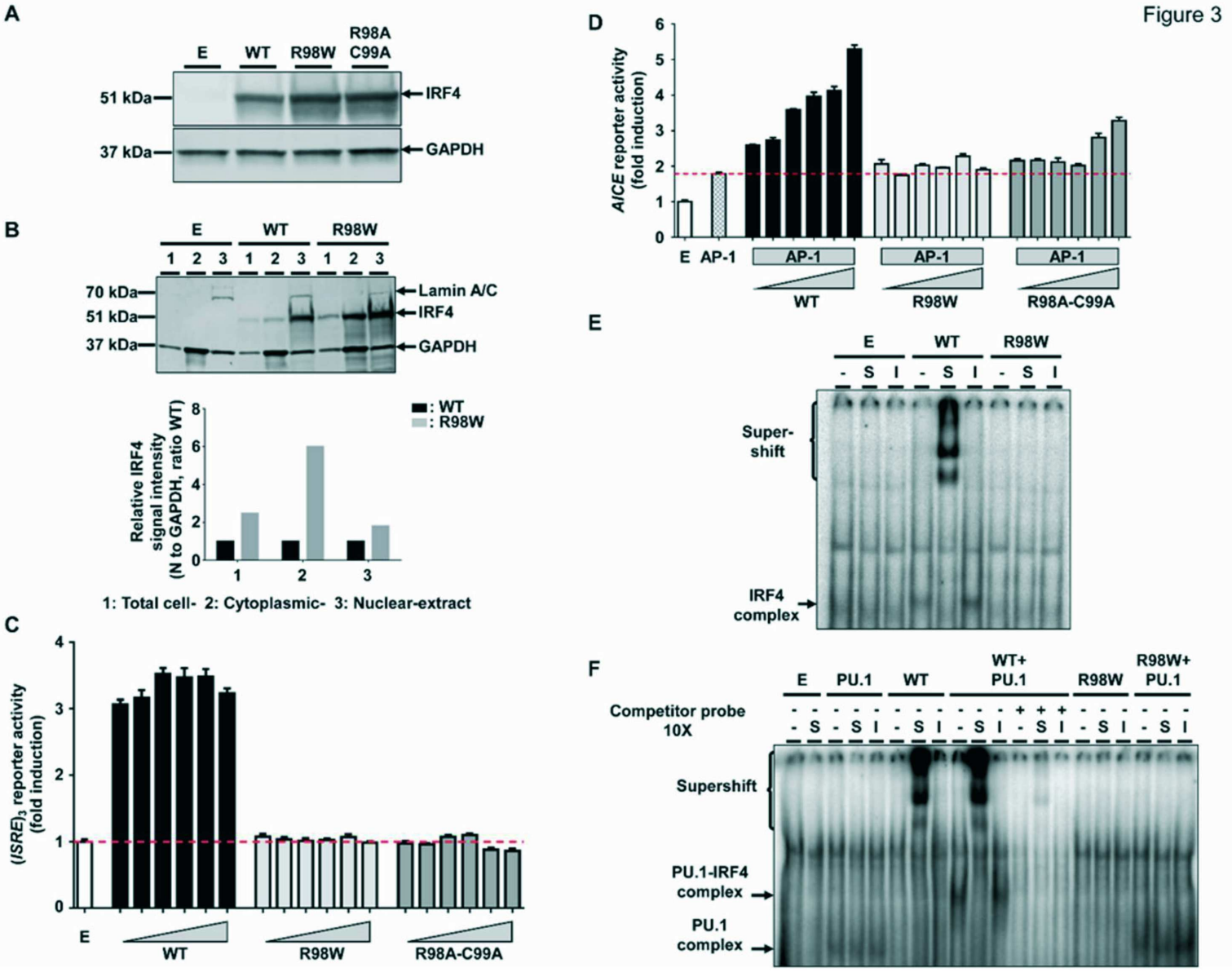
A
E
WT
R98W
R98A C99A
51 kDa
IRF4
37 kDa
GAPDH
B
E
WT
R98W
1 2 3 1 2 3 1 2 3
70 kDa
51 kDa
37 kDa
Lamin A/C
IRF4
GAPDH
: WT
: R98W
Relative IRF4 signal intensity (N to GAPDH, ratio WT)
1: Total cell- 2: Cytoplasmic- 3: Nuclear-extract
C
(ISRE)3 reporter activity (fold induction)
E
WT
R98W
R98A-C99A
D
A/CE reporter activity (fold induction)
E
AP-1
WT
R98W
R98A-C99A
E
E
WT
R98W
- S I - S I - S I
Super-shift
IRF4 complex
F
E
PU.1
WT
WT+ PU.1
R98W
R98W+ PU.1
Competitor probe 10X
Supershift
PU.1-IRF4 complex
PU.1 complex

Figure 3-figure supplement 1

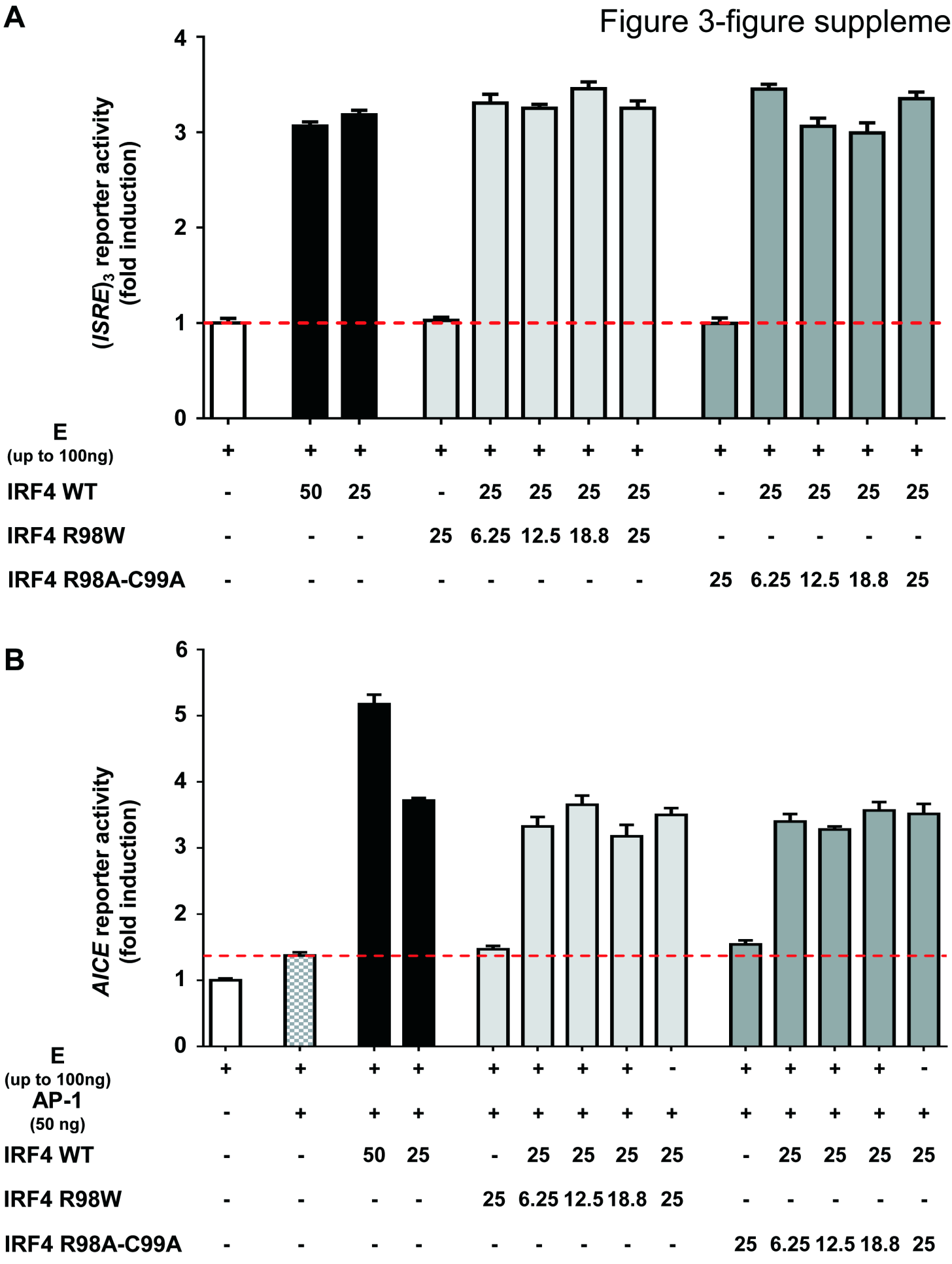

Figure 3-figure supplement 2

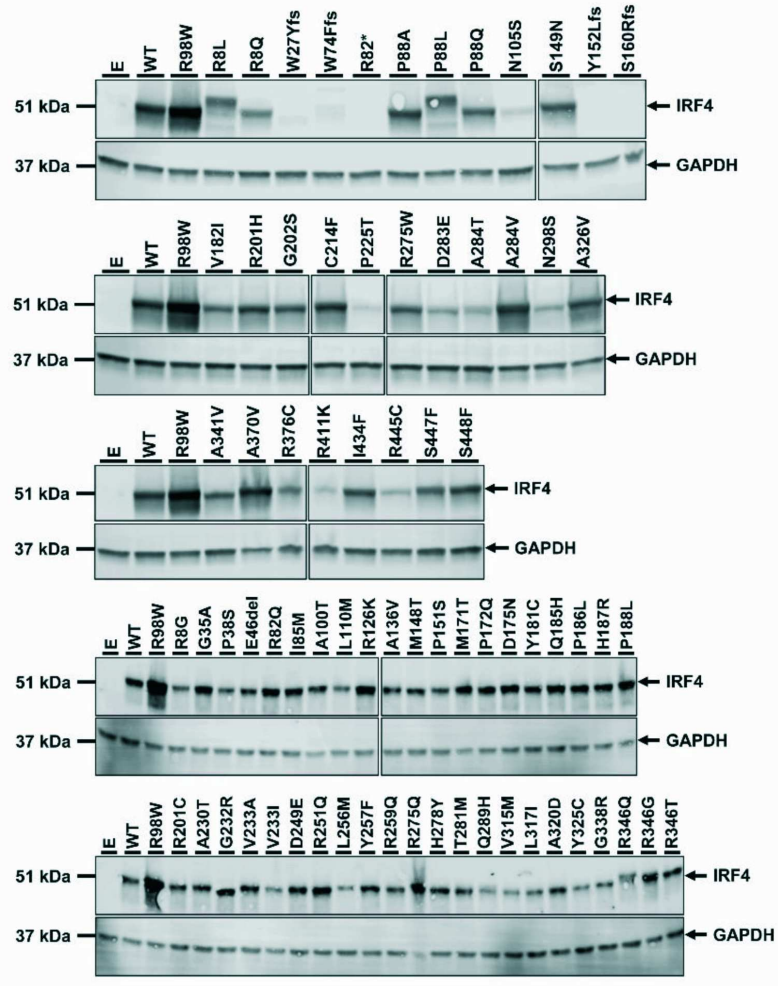

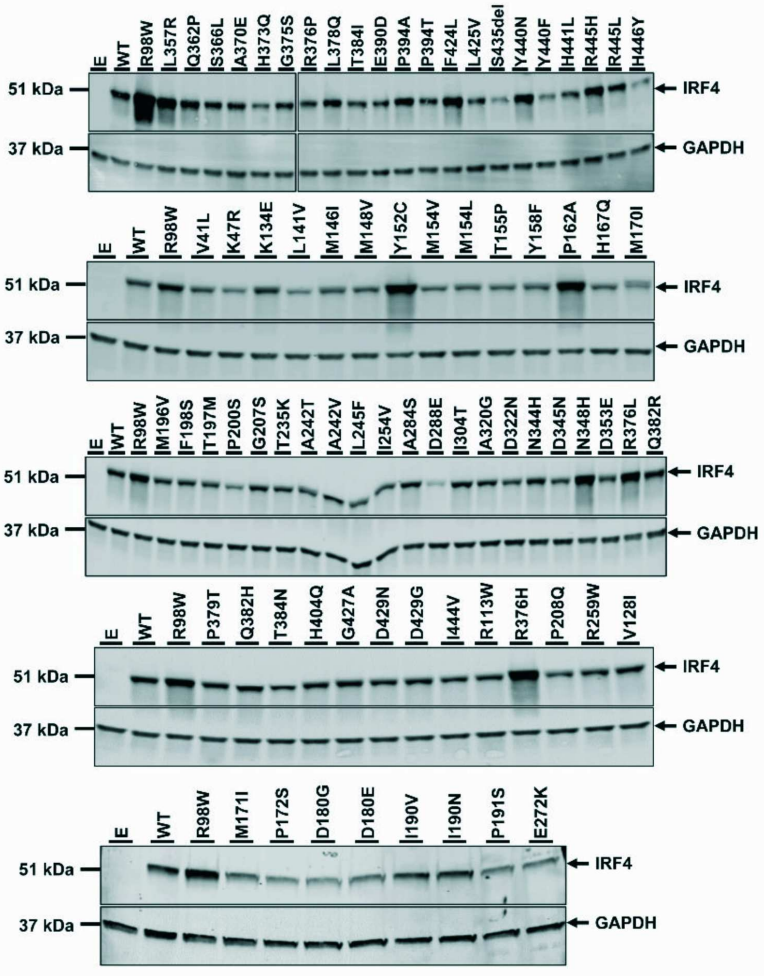

Figure 3-figure supplement 3

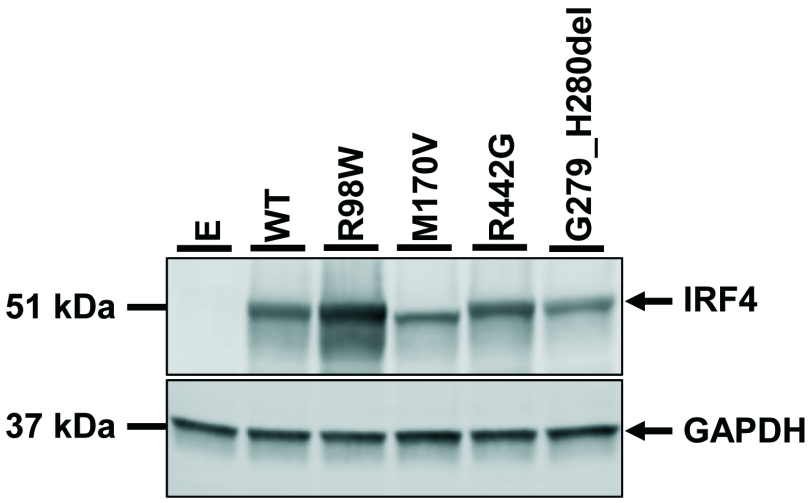

Figure 3-figure supplement 4

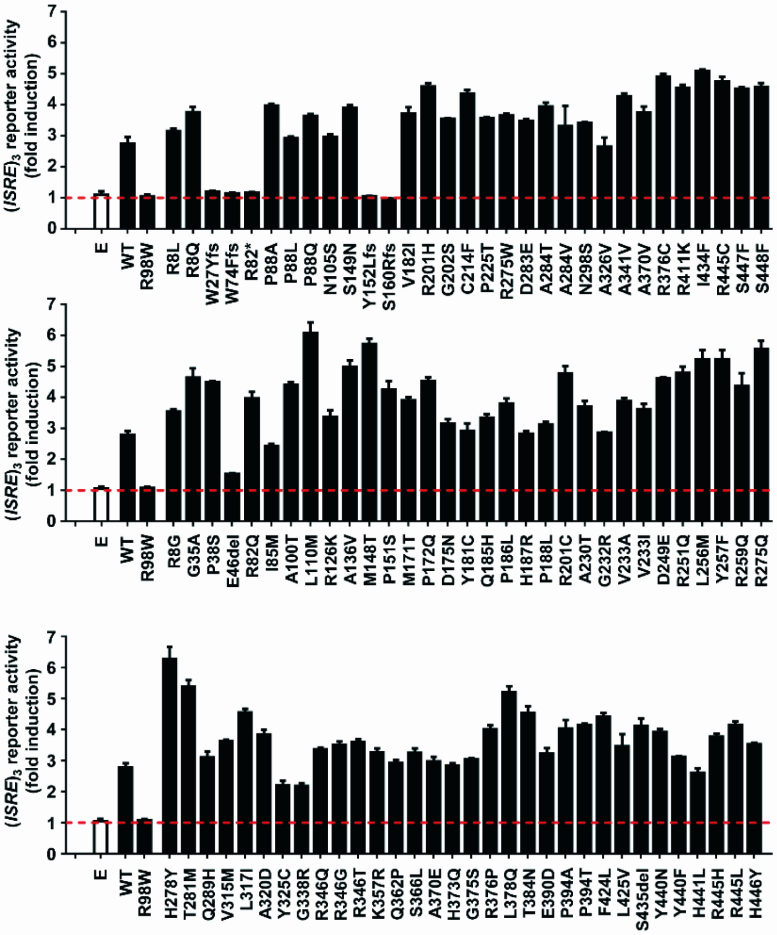

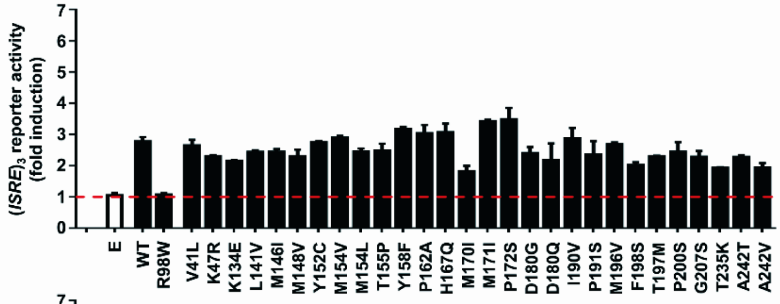

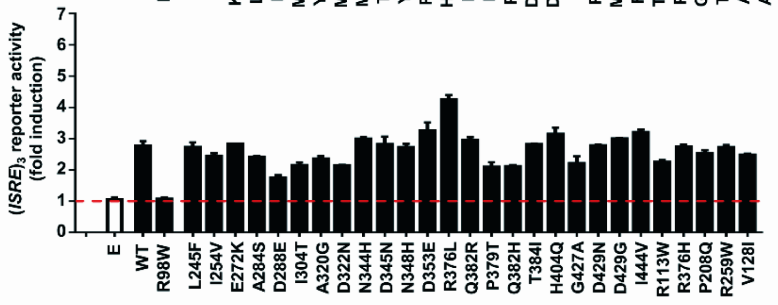

Figure 3-figure supplement 5

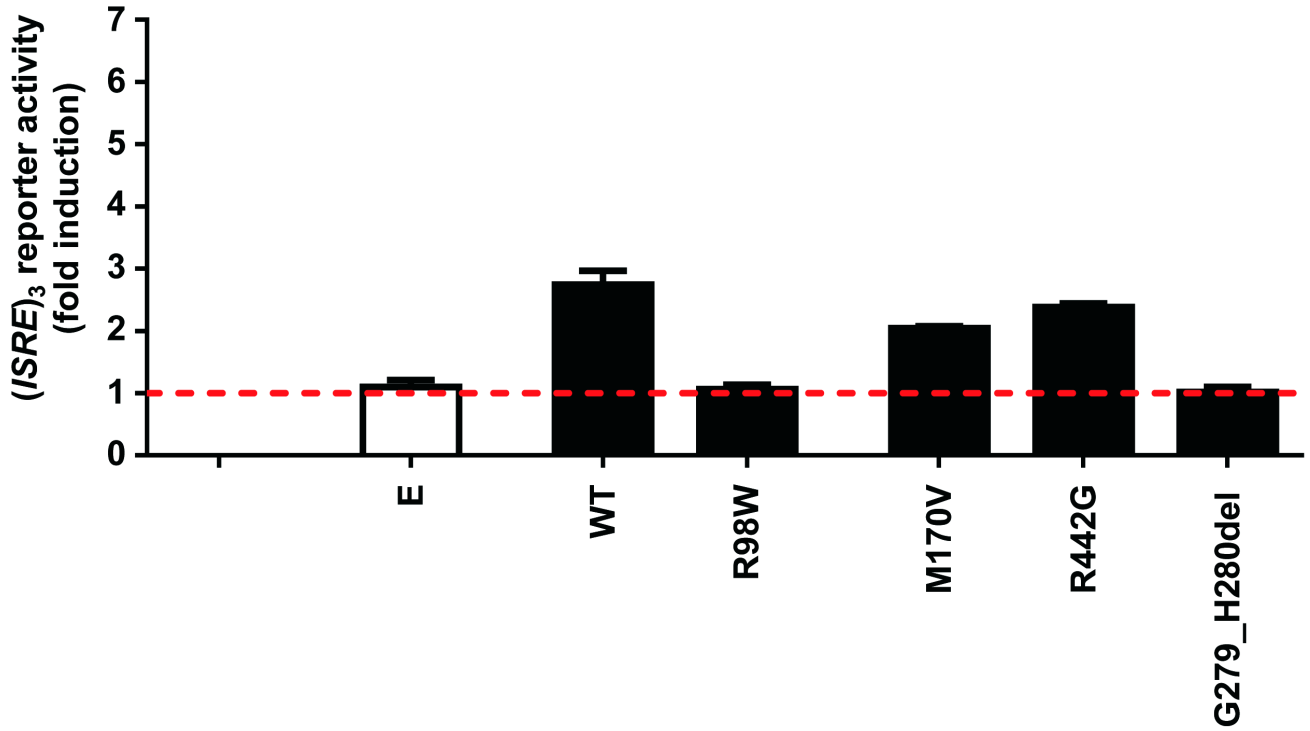

Figure 4

A

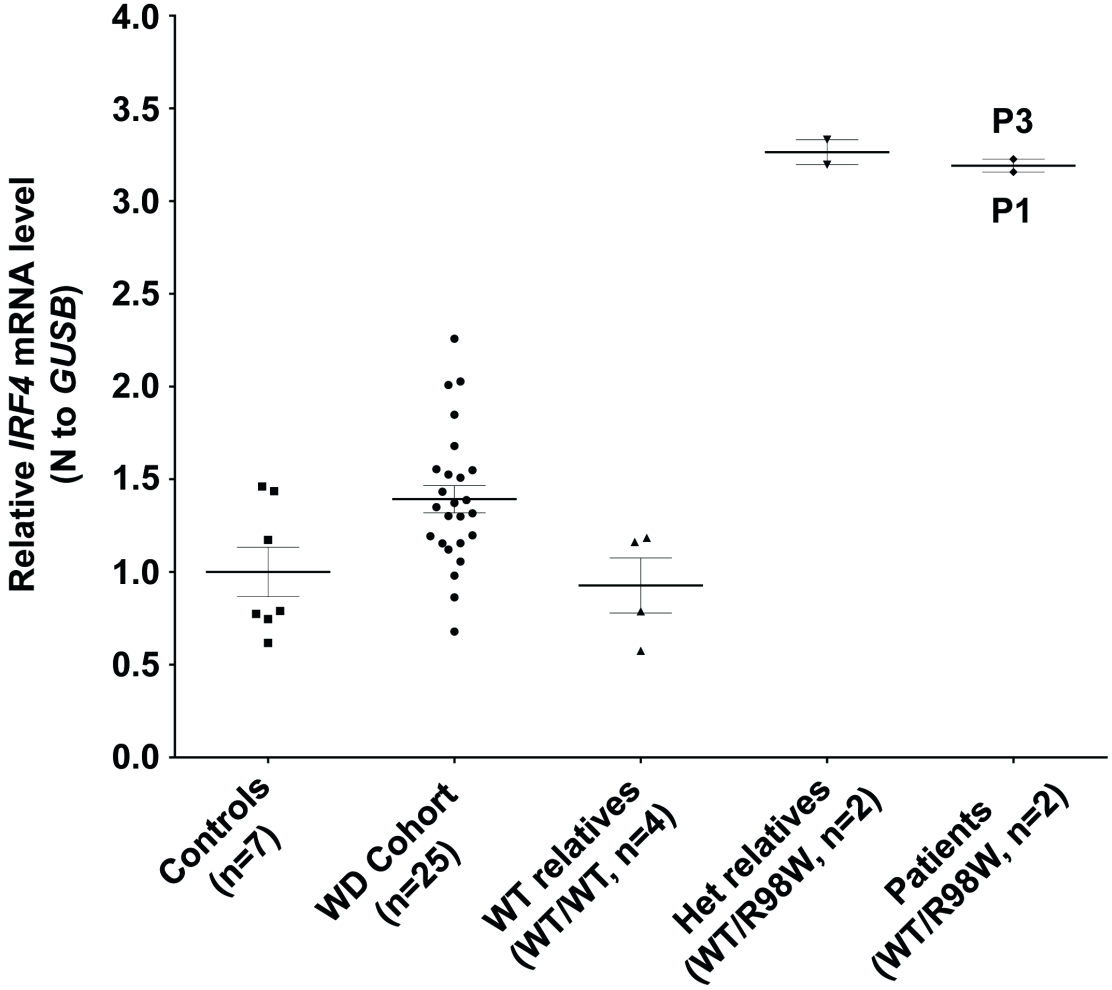

B

	WT allele (%)	R98W allele (%)
Controls (n=2)	100	0
WT relative	100	0
Het relative	43.3	56.7
P1	51.9	48.1
P3	40	60

Figure 4-figure supplement 1

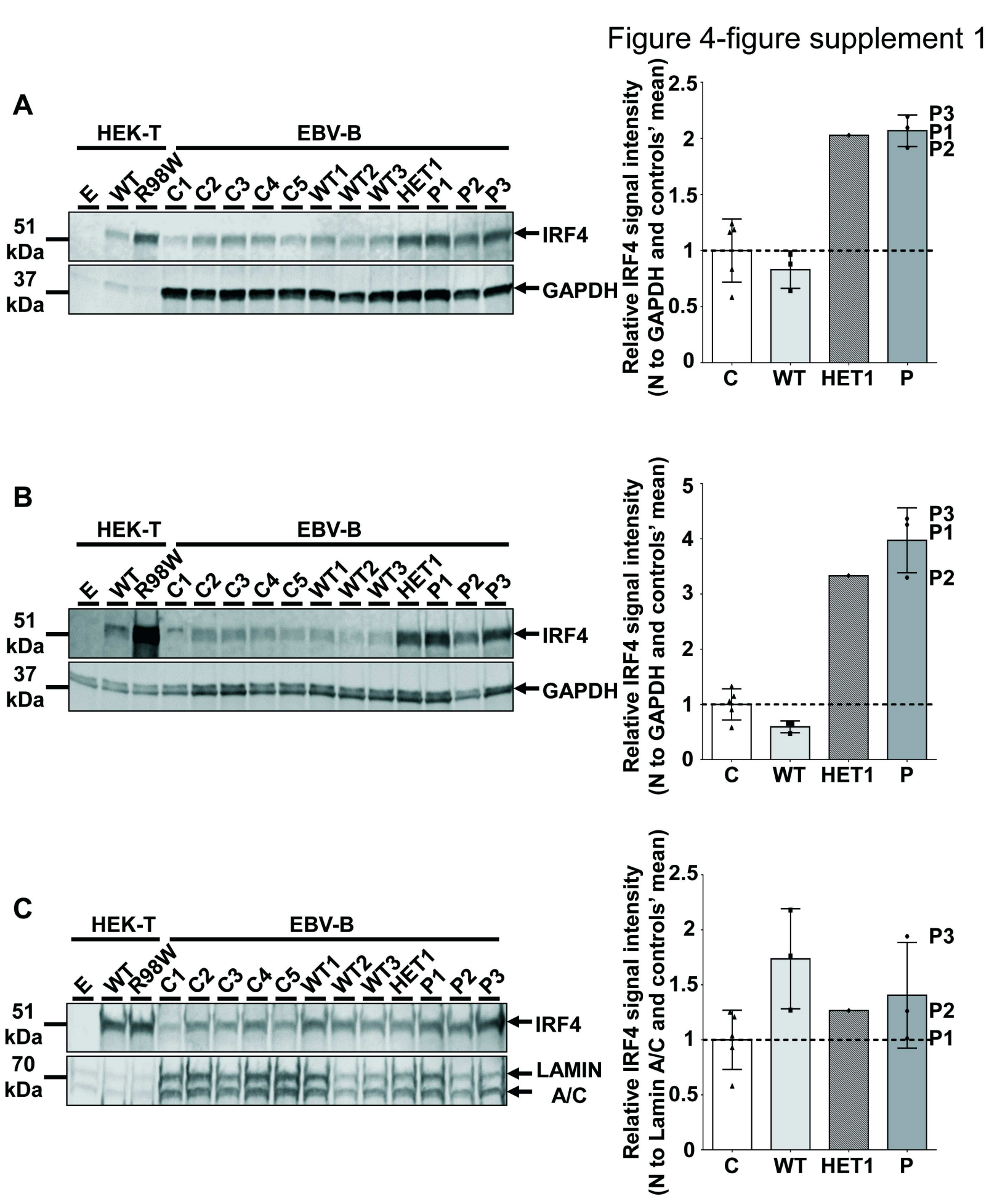

Figure 5

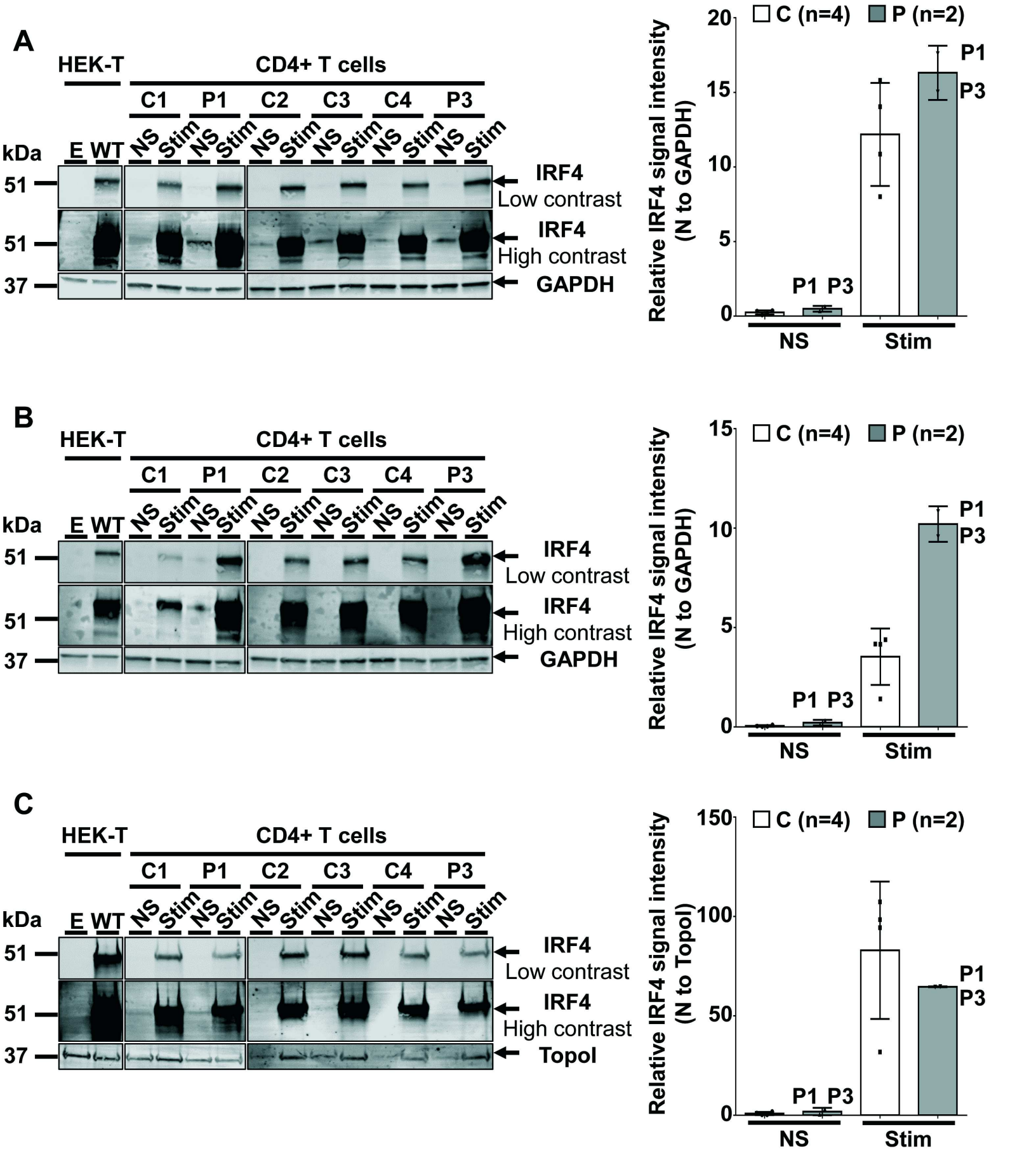
A
HEK-T
CD4+ T cells
C1
P1
C2
C3
C4
P3
kDa
E WT
NS
Stim
51
51
37
IRF4
Low contrast
IRF4
High contrast
GAPDH
Relative IRF4 signal intensity
(N to GAPDH)
C (n=4)
P (n=2)
20
15
10
5
0
P1
P3
NS
Stim
B
HEK-T
CD4+ T cells
C1
P1
C2
C3
C4
P3
kDa
E WT
NS
Stim
51
51
37
IRF4
Low contrast
IRF4
High contrast
GAPDH
Relative IRF4 signal intensity
(N to GAPDH)
C (n=4)
P (n=2)
15
10
5
0
P1
P3
NS
Stim
C
HEK-T
CD4+ T cells
C1
P1
C2
C3
C4
P3
kDa
E WT
NS
Stim
51
51
37
IRF4
Low contrast
IRF4
High contrast
Topol
Relative IRF4 signal intensity
(N to Topol)
C (n=4)
P (n=2)
150
100
50
0
P1
P3
NS
Stim

Figure 5-figure supplement 1

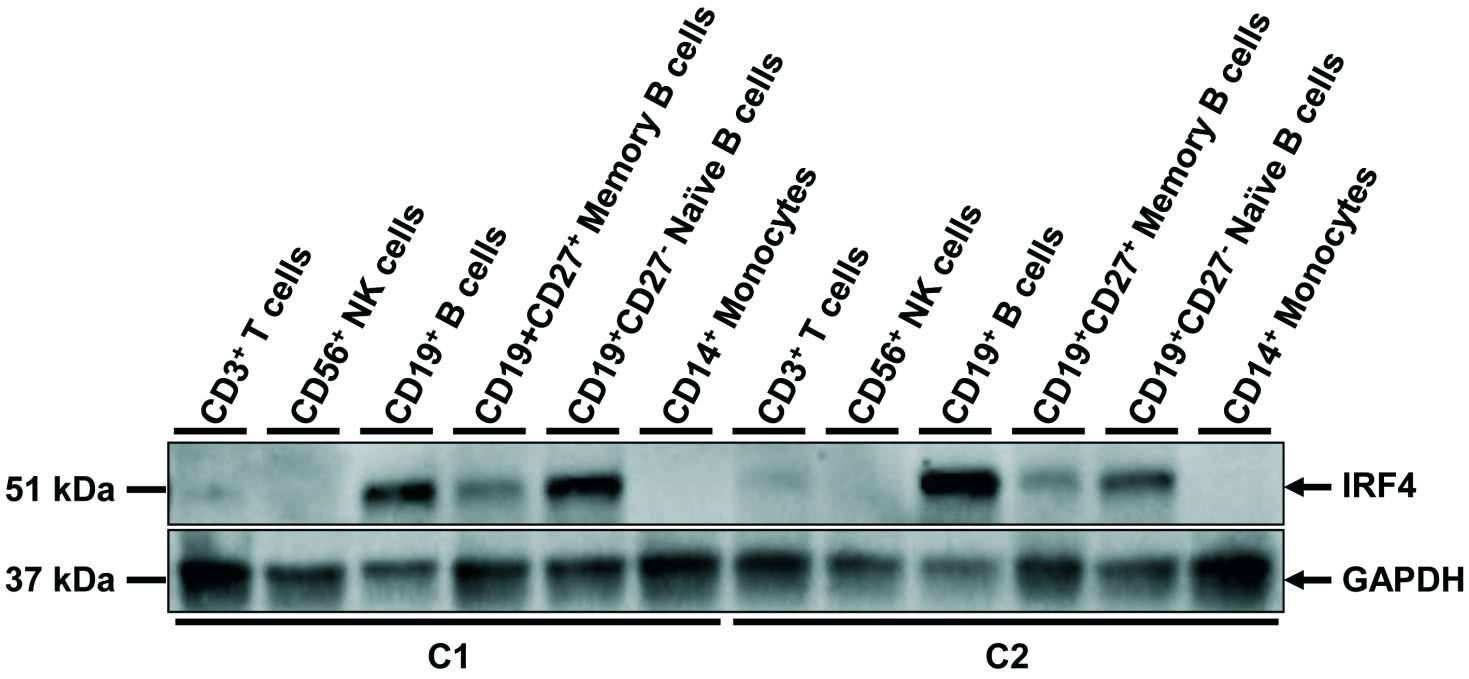

Figure 5-figure supplement 2

A

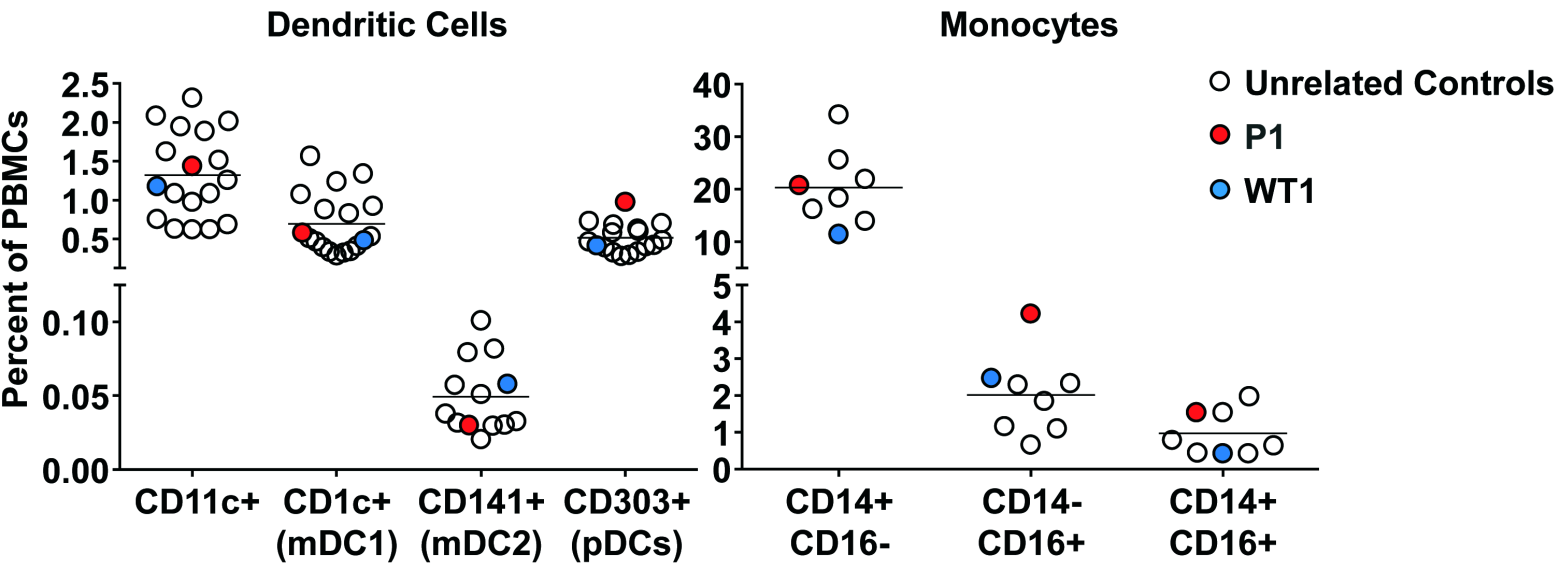

B

Gating Strategy

Population	Characterization
mDC1	HLA-DR+, CD14-, CD16-, Lin (CD3, CD15, CD19, CD56, NKp46)-, CD11c+, CD141-, **CD1c+**
mDC2	HLA-DR+, CD14-, CD16-, Lin (CD3, CD15, CD19, CD56, NKp46)-, CD11c+, **CD141+**, CD1c-
pDCs	HLA-DR+, CD14-, CD16-, Lin (CD3, CD15, CD19, CD56, NKp46)-, **CD303+**
CD14+ CD16- Monocytes	HLA-DR+, Lin (CD3, CD15, CD19, CD56, NKp46)-, **CD14+, CD16-**
CD14- CD16+ Monocytes	HLA-DR+, Lin (CD3, CD15, CD19, CD56, NKp46)-, **CD14-, CD16+**
CD14+ CD16+ Monocytes	HLA-DR+, Lin (CD3, CD15, CD19, CD56, NKp46)-, **CD14-, CD16+**

Figure 5-figure supplement 3

A

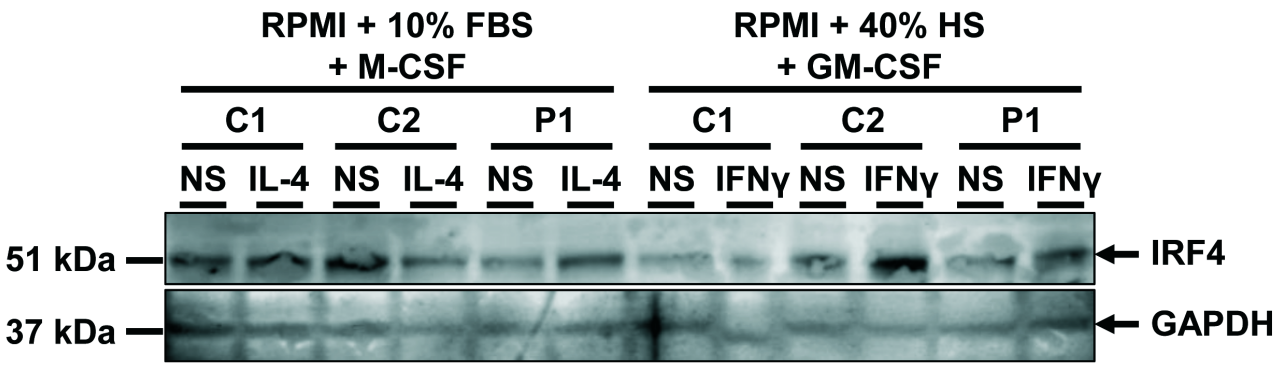

B

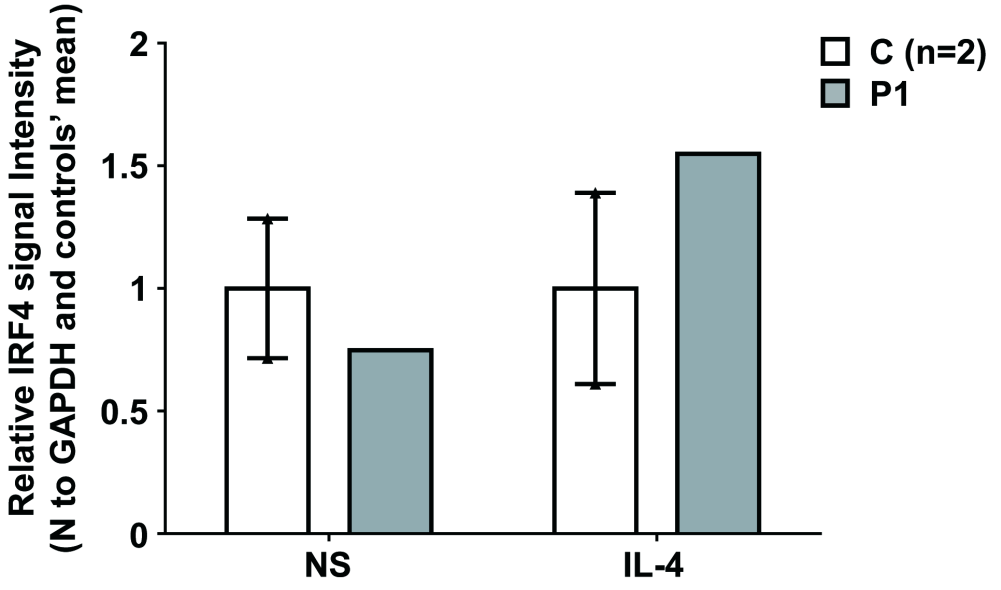

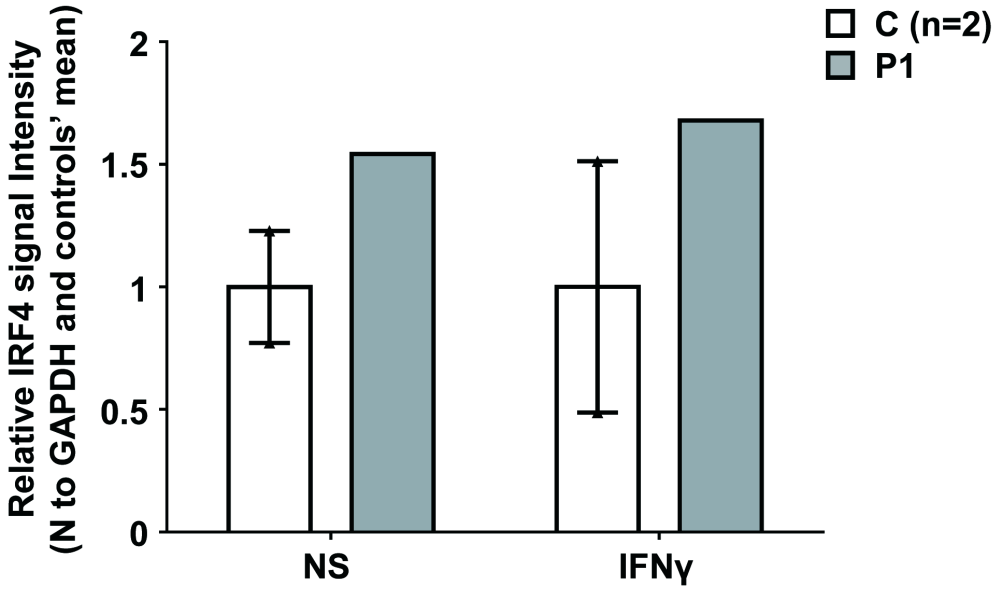

Figure 5-figure supplement 4

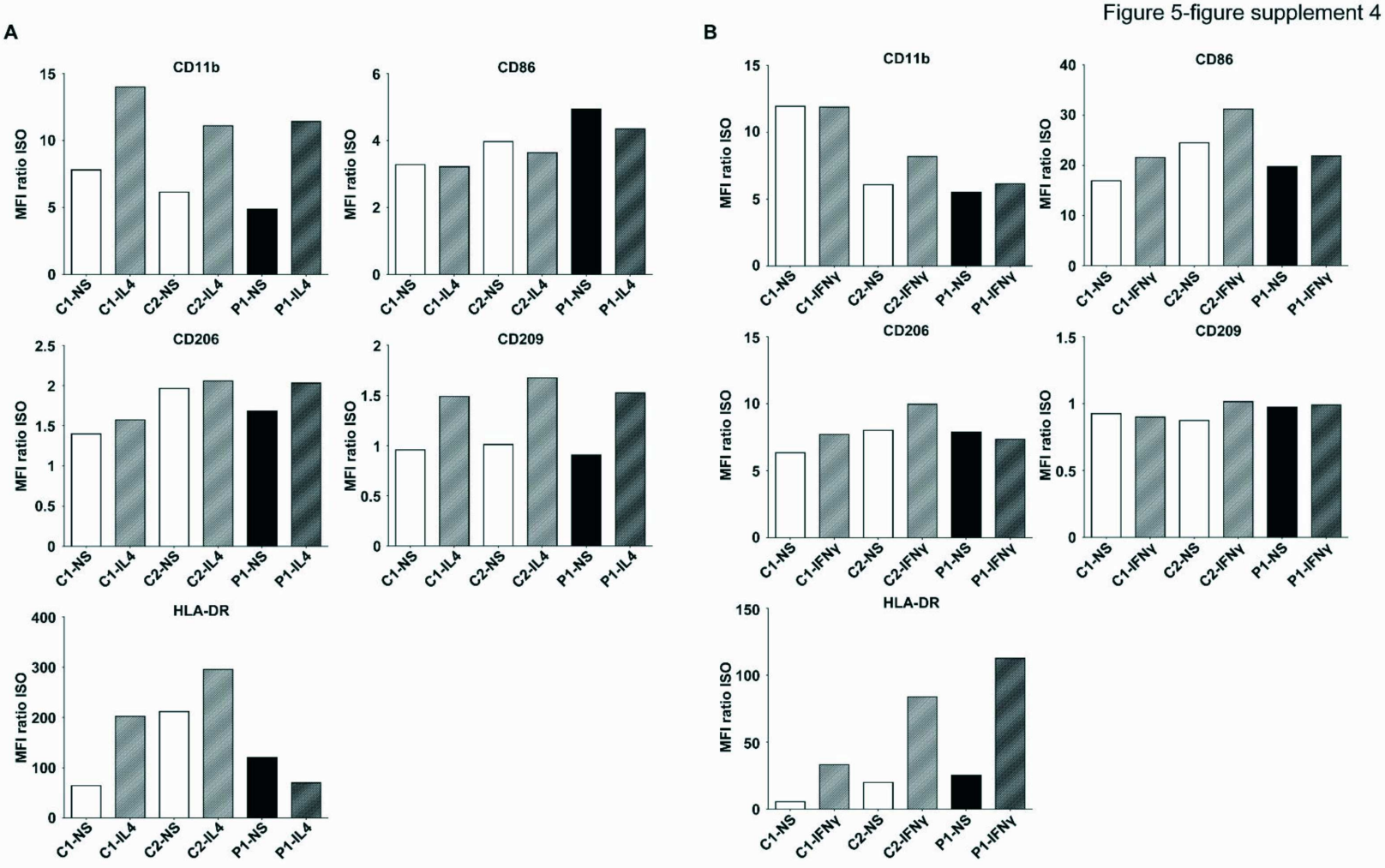

Figure 5-figure supplement 5

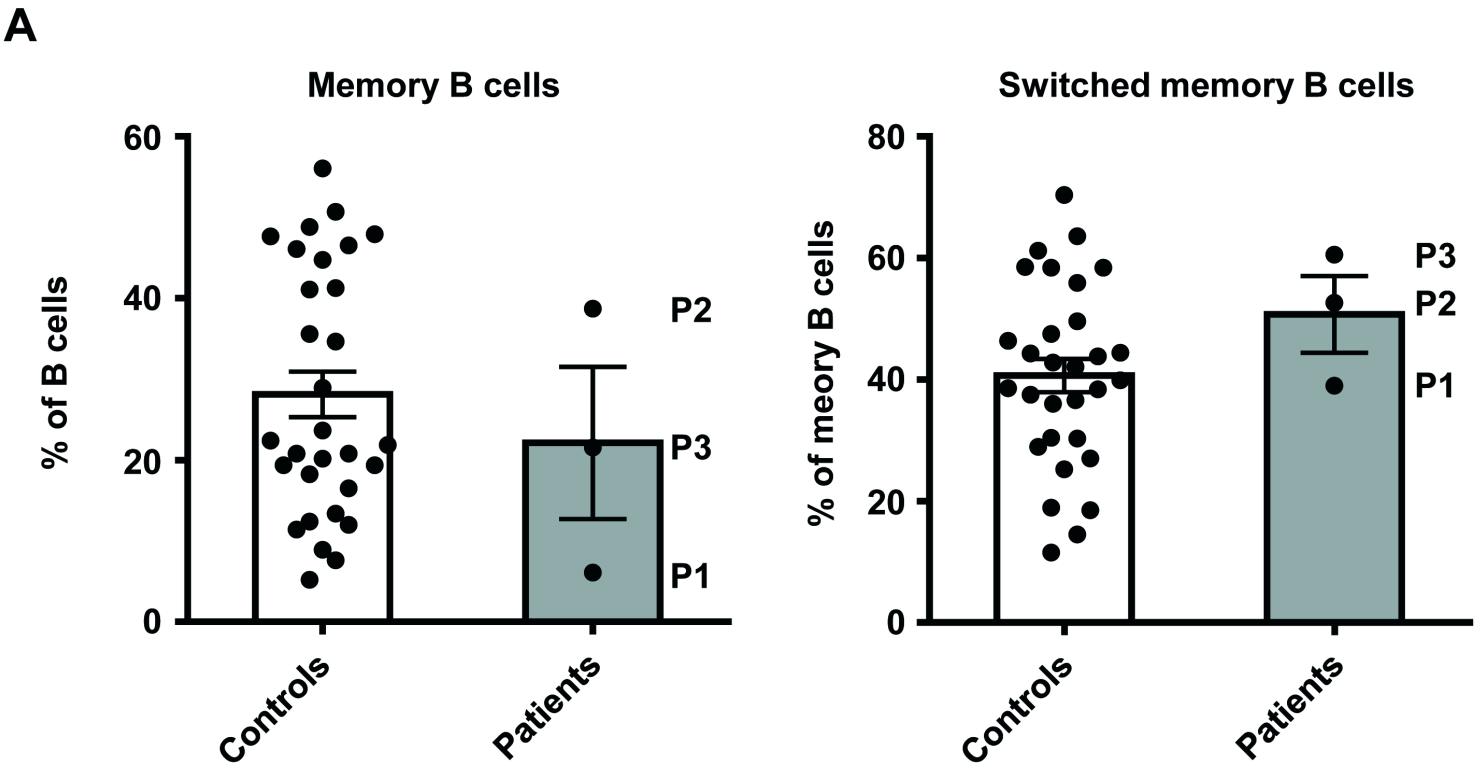

Figure 5-figure supplement 6

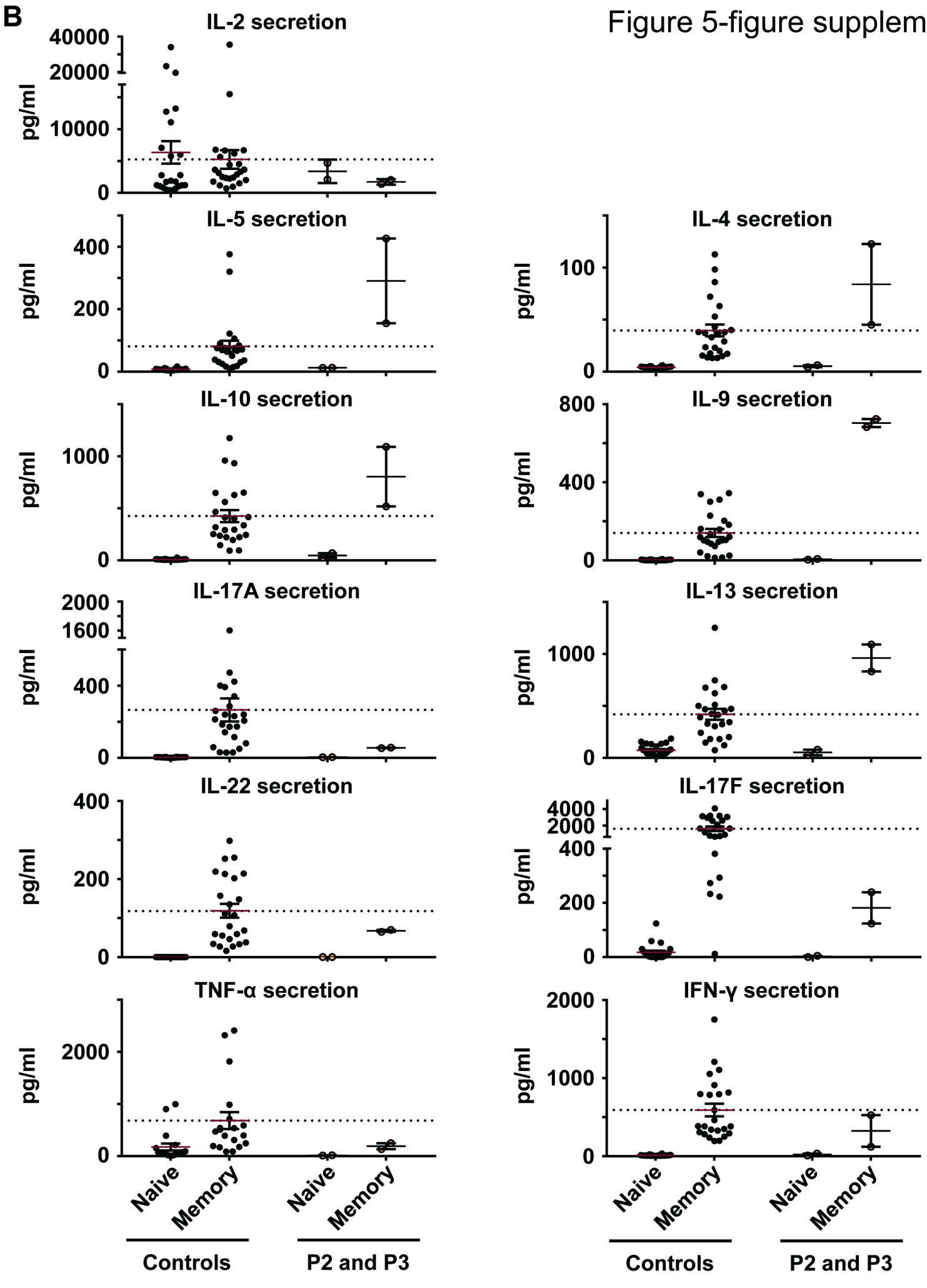

C

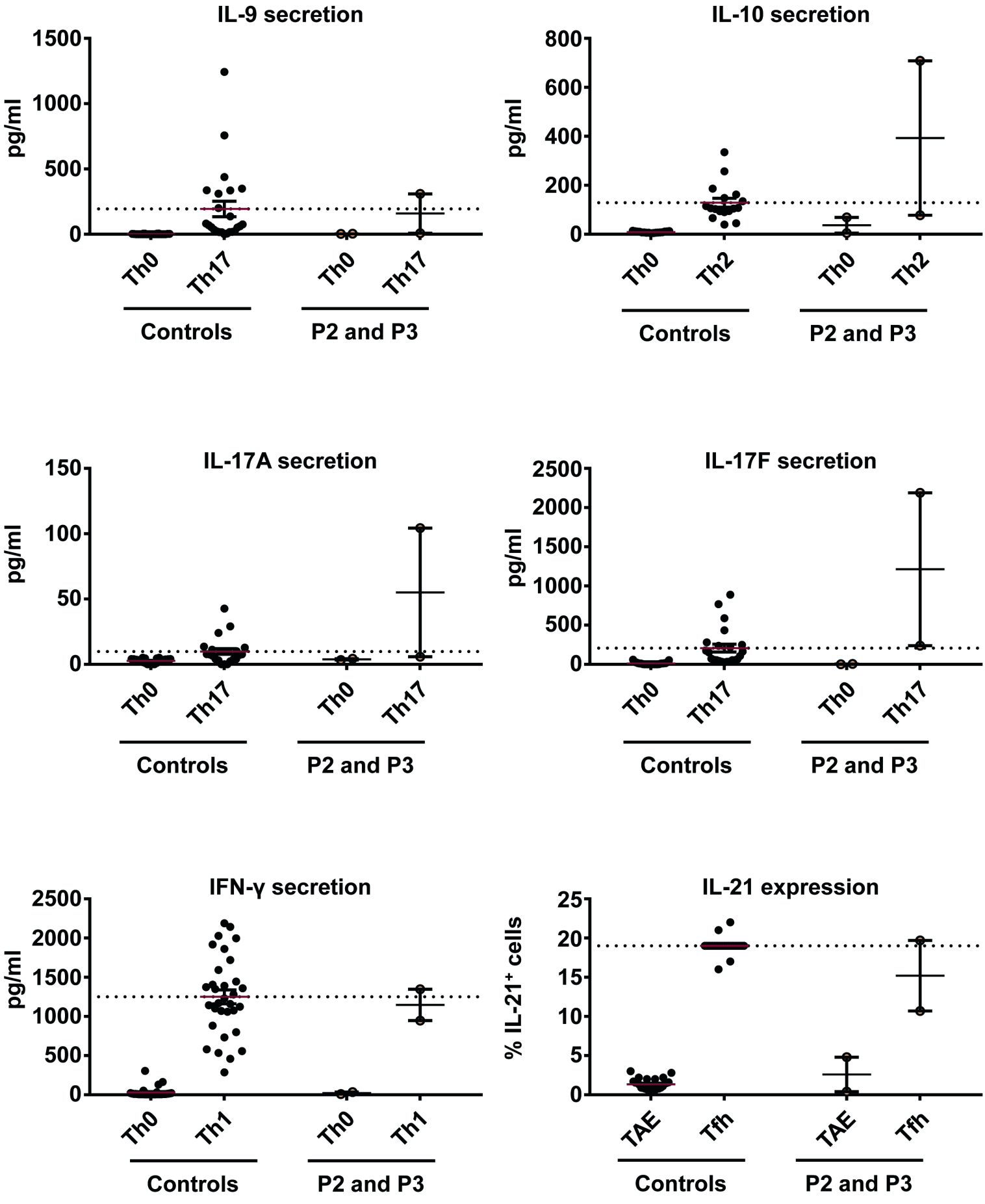
IL-9 secretion
pg/ml
1500
1000
500
0
Th0
Th17
Th0
Th17
Controls
P2 and P3
IL-10 secretion
pg/ml
800
600
400
200
0
Th0
Th2
Th0
Th2
Controls
P2 and P3
IL-17A secretion
pg/ml
150
100
50
0
Th0
Th17
Th0
Th17
Controls
P2 and P3
IL-17F secretion
pg/ml
2500
2000
1500
1000
500
0
Th0
Th17
Th0
Th17
Controls
P2 and P3
IFN-γ secretion
pg/ml
2500
2000
1500
1000
500
0
Th0
Th1
Th0
Th1
Controls
P2 and P3
IL-21 expression
% IL-21+ cells
25
20
15
10
5
0
TAE
Tfh
TAE
Tfh
Controls
P2 and P3

Figure 6

A

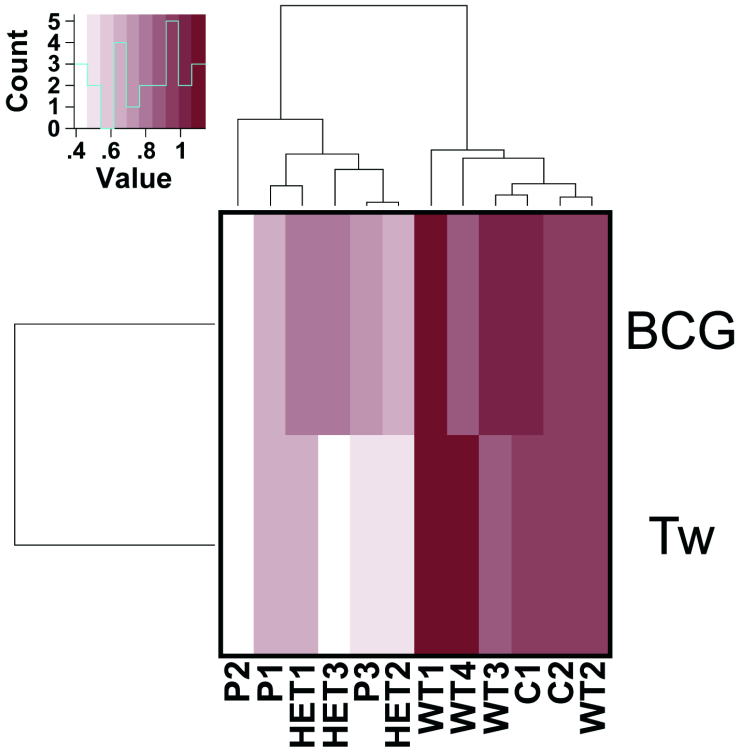
Count
5
4
3
2
1
0
.4 .6 .8 1
Value
BCG
Tw
P2
P1
HET1
HET3
P3
HET2
WT1
WT4
WT3
C1
C2
WT2

B

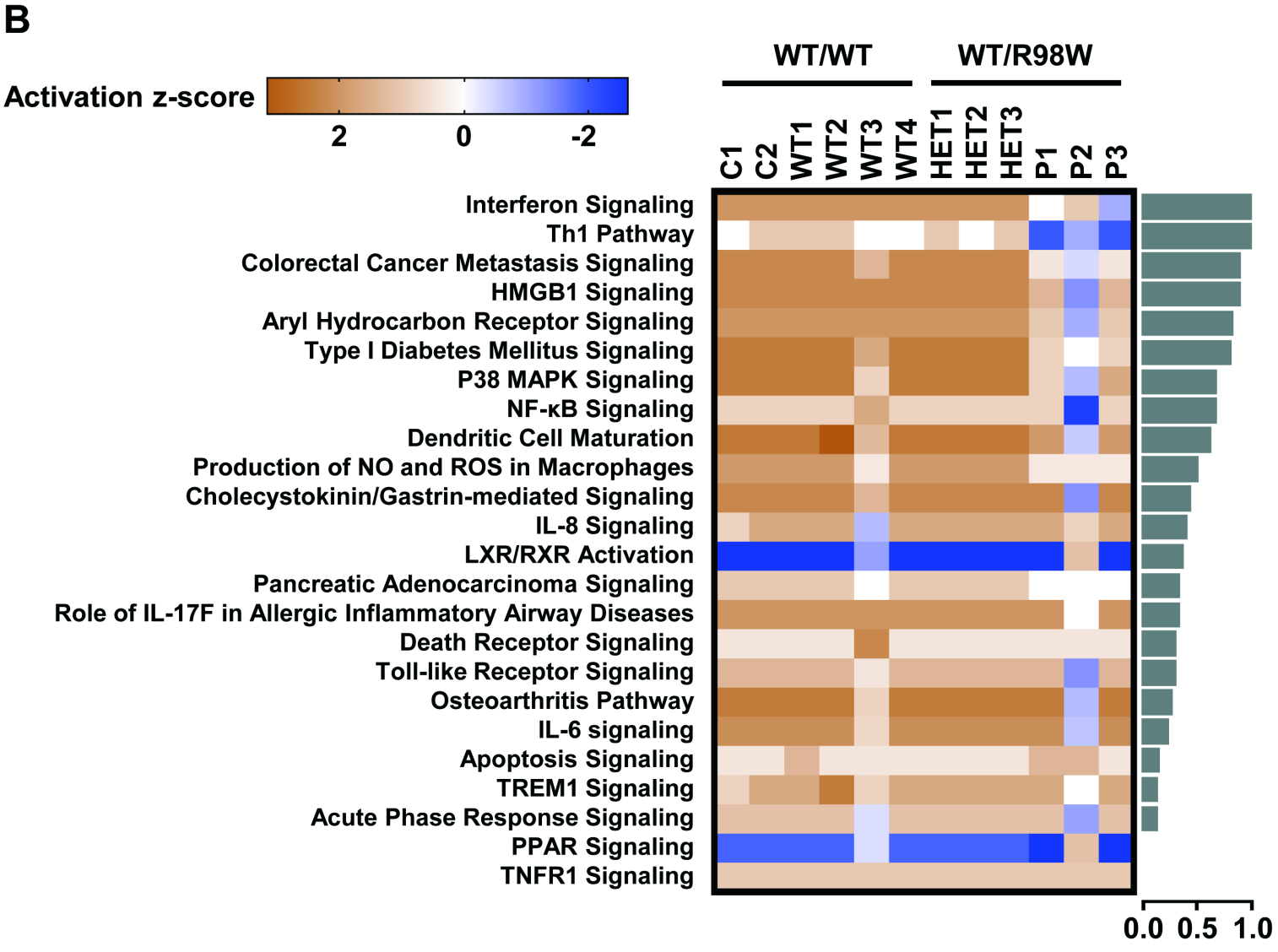
Activation z-score
2
0
-2
WT/WT
WT/R98W
C1
C2
WT1
WT2
WT3
WT4
HET1
HET2
HET3
P1
P2
P3
Interferon Signaling
Th1 Pathway
Colorectal Cancer Metastasis Signaling
HMGB1 Signaling
Aryl Hydrocarbon Receptor Signaling
Type I Diabetes Mellitus Signaling
P38 MAPK Signaling
NF-κB Signaling
Dendritic Cell Maturation
Production of NO and ROS in Macrophages
Cholecystokinin/Gastrin-mediated Signaling
IL-8 Signaling
LXR/RXR Activation
Pancreatic Adenocarcinoma Signaling
Role of IL-17F in Allergic Inflammatory Airway Diseases
Death Receptor Signaling
Toll-like Receptor Signaling
Osteoarthritis Pathway
IL-6 signaling
Apoptosis Signaling
TREM1 Signaling
Acute Phase Response Signaling
PPAR Signaling
TNFR1 Signaling
0.0 0.5 1.0